Studying Specific Ion Effects at the Silica/Aqueous Interface

by

Sun Kim

A thesis submitted in partial fulfillment of the requirements for the degree of

Master of Science

Department of Chemistry
University of Alberta

© Sun Kim, 2017

Abstract

Nonlinear optical techniques are widely used for surface analysis, as they are surface specific and can be used to probe interfaces of insulators such as silica. Silica is commonly found in nature such as reservoirs of natural water and oils. Nonetheless, it is not clear how silica interacts with the water at a molecular level. In this thesis, second harmonic generation (SHG) and sum frequency generation (SFG) techniques were used to probe silica/aqueous interface under different environmental conditions. Firstly, broadband vibrational SFG spectroscopy was used to study specific ion effects (SIEs) and investigate how different ions affect the ordering of interfacial water molecules at the silica/aqueous interface as a function of pH. SFG spectra were measured for 0.5 M CsCl, KCl, NaCl and LiCl from pH 2-12 to specifically study the pH-dependent effect of monovalent cations on the interfacial water structure at a silica surface. SFG results show that at neutral pH~ 7.0, Cs^+ and K^+ adsorb more strongly than Li^+ and Na^+, following the direct Hofmeister series. The reverse Hofmeister trend was observed when pH was greater than 10 where Li^+ had the greatest adsorption and Cs^+ had the least adsorption. The results show that cation adsorption is dependent on the type of ions as well as the pH of the solution. Secondly, broadband vibrational SFG spectroscopy and non-resonant SHG spectroscopy were used to investigate the effect of 0.1 M $NaHCO_3$, one of the most commonly found salts in natural water and in industrial water used in oil sands. SFG and SHG of 0.1 M $NaHCO_3$ were compared with 0.1 M NaCl, a salt which has been previously investigated by our group. SFG results show that HCO_3^- anions likely partition within diffuse layer towards siloxide-Na^+ coordinated surface rather than directly adsorbing to silica surface. Overall, both of SIEs

results could be used to better understand many environmental, geochemical and industrial processes and applied in modeling of pollutant transport in water treatment.

Preface

This thesis is an original work by Sun Kim. Some of the research conducted for this thesis forms part of a collaboration with other group members, which will be stated later.

Chapter 2 of this thesis is in a manuscript that has recently been submitted as DeWalt-Kerian, E. L.; Kim, S.; Azam, M. S.; Zeng, H.; Liu, Q.; Gibbs, J. M., pH-Dependent Inversion of Hofmeister Trends in the Water Structure of the Electrical Double Layer. *J. Phys. Chem. Lett.* **2017**, 2855-2861. Both Dr. Kerian and I were responsible for the data collection and analysis. Dr. Kerian was responsible for the final manuscript composition. Dr. Julianne Gibbs was the supervisory author.

Chapter 3 of this thesis is an original work by me. No part of this chapter has been previously published. I was responsible for the data collection and analysis. All the SFG spectra were collected by me. Part of the SHG spectra were collected by Dr. Darlington.

Acknowledgement

Firstly, I would like to express my sincere gratitude to my supervisor Dr. Julianne Gibbs for all her help, guidance, and precious advice throughout my graduate career. I feel honored and privileged to be a member of the Gibbs research group at the University of Alberta.

I would like to acknowledge my defence examination committee members and committee members: Dr. Yunjie Xu, Dr. Charles Lucy, and Dr. Sarah Styler. I appreciated your valuable suggestions to improve my research.

I would also like to thank all my colleagues in the Gibbs group, especially Dr. Kerian, Dr. Darlington, Dr. Li and past group member Dr. Shafiul Azam. Thank you for your kind help and support.

Finally, I would like to thank all my friends especially Hongbiao Tao and Hye Lin Kim for their encouragement and support. I would also like to thank my parents Eun Mi Lee and Young Joon Kim for their support.

Table of Contents

List of Figures

Chapter 1

Introduction

1.1. The Importance of the Silica/Aqueous Interface

Silica is one of the most abundant elements found in the earth's crust and can exist in many forms including quartz and amorphous silica.[2] Silica is also the main component of sand, present in primarily quartz form. Upon contacting with water, a layer of amorphous silica with silanol groups (-SiOH) forms on the surface of quartz.[2] Silica has a point of zero charge around pH 2 in pure water. As pH is increased above the point of zero charge, the silica surface will become more negatively charged as the silanol groups (-SiOH) become deprotonated and form siloxides ($-SiO^-$).[3]

Many geological and environmental processes such as dissolution, weathering, and adsorption occur at the surface of silica thereby making the structure of silica/aqueous interface relevant in many environmental and geological applications.[2, 4] Depending on the environmental conditions such as pH and composition of salts, the interactions between the silica surface and water can vary greatly. Understanding these changes in the interactions under different salt and pH condition can aid industrial processes such as improving the separation of bitumen from silica sands during the extraction of oil sands as well as developing a method for dewatering oil sands tailings by controlling the adsorption processes between silica and specific ions.[2, 4-8]

In this thesis, specific ion effects (SIE) on the silica/aqueous interface are examined using sum frequency generation (SFG) and second harmonic generation (SHG) techniques. A specific ion effects (SIE) is an effect that depends on the ion identity. For example, when K^+ made the surface more acidic than Na^+, it would be considered specific ion effects. In this chapter, I will give a general introduction of the thesis and focus on the nature of the electrical double layer formed at a charged surface in aqueous solution, the Hofmeister series of ions and its relationship

to water structure. General theoretical descriptions of non-linear optics and SHG and SFG techniques used for analysis will be also be discussed. In addition, a summary of previous studies aimed at understanding the role of cations on the behavior of the silica/water interface will be provided. Chapter 2 will discuss the effect of monovalent cations on the ordering of interfacial water molecules and acid-base chemistry of silica using vibrational SFG spectroscopy and relate each property of ions such as size and hydration shell to its interactions with water and silica. Chapter 3 will investigate the possible effect of bicarbonate, an ion that is commonly found in natural water, on the silica/aqueous interface using SHG and SFG techniques.

1.2. Electrical Double Layer

In order to fully understand water structure at the water-silica interface, it is first important to understand the electrical double layer (EDL) that forms at the interface of charged surfaces and aqueous solutions.[9-14] There are many different models that describe the structure of the electrical double layer. The model that is commonly used to for the silica/aqueous interface is the Gouy-Chapman-Stern-Grahame (GCSG) model as shown in Figure 1.1.[9, 15] In this model, the electrical double layer consists of a compact layer (also known as the Stern layer) and a diffuse layer.[9, 11] In the Stern layer, a charged surface (0-plane) is present and the ions that are opposite in charge to that surface are attracted to the surface. This accumulation of counter ions near the surface creates a layer of charge (d-plane). This d-plane is also known as the outer Helmholtz plane (OHP). Within the Stern layer, the surface potential drops linearly as the charged surface and counter-ions (at 0-plane and d-plane) act as a parallel capacitor. In the diffuse layer, there is a distribution of counter-ions and co-ions such that potential drops exponentially. In the bulk

solution where the potential drops to zero, there is an equal distribution of counter-ions and co-ions.

The interfacial potential (Φ_0) is the potential at the 0-plane shown in Figure 1.1 and is determined by the amount of charge present at the surface as well as the type of the ions that are present near the surface.[9] In the case of the silica/aqueous interface, ions are drawn to the interface differently due to their unique hydration and size/charge ratio. Accordingly, this varying interaction between the ion and the surface will yield different surface charge densities and interfacial potentials at silica surface.[8] The influence of specific ions on the amount of ordered water due to changes in the interfacial potential at the silica/aqueous interface under a wide range of pH environments will be discussed in Chapter 2.

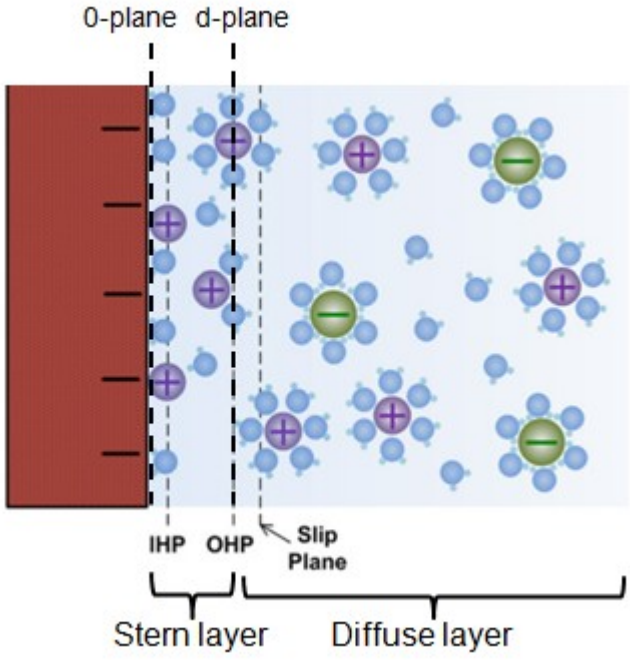

Figure 1.1. Gouy-Chapman-Stern-Grahame (GCSG) model of the electrical double layer at a negatively charged surface.[16] Blue circles denote water molecules. This diagram was adopted from the reference 16, which illustrated the GCSG model.

1.3. Hofmeister Series

In 1877, Franz Hofmeister first ordered anions in terms of their ability to precipitate egg white protein. Hofmeister then ordered anions and cations in terms of their ability to "salt in" proteins which means the ability to increase solubility of protein in solution as well as make it less stable i.e. cause it to denature.[17-23] In the case of protein, anions were shown to have larger effects than cations.[17, 23-25] These ions can be further categorized into their abilities to reinforce or disrupt the hydrogen bonding structure of water: kosmotropic ions ("structure makers") and chaotropic ions ("structure breakers"). For the anionic trend $F^-<Cl^-<Br^-<I^-$, kosmotropic anions tend to be small in size, well-hydrated and tend to "salt out" proteins whereas chaotropic anions (right side of the trend) tend to be big in size, have small hydration shell layer and have "salt in" effects. The strongly hydrated kosmotropic anions are assumed to have a greater number of water molecules around the ion, which take away water molecules from the protein causing a salting-out of proteins (ie. they become insoluble).[25-26] On the other hand, weakly hydrated chaotropic anions are assumed to have fewer number of water molecules around the ion due to their water structure breaking properties and therefore make water molecules interact more with proteins causing proteins to "salt-in" as a result of their greater hydration shells.[25-26] However, the opposite trend is observed for cations where chaotropic cations, which are big and have a small hydration water shell cause "salting-out" effects and kosmotropic cations (right side of trend) are small and have big hydration shells cause "salting-in" effects on proteins: $Cs^+<K^+<Na^+<Li^+$. Moreover, depending on the net charge of the protein and its functional groups, Hofmeister series could reverse.[25, 27] Hofmeister series was also shown to reverse depending on the surface charge and surface polarity,[28-29] which suggests that both the

environmental conditions of solution and the surface condition matters with having specific trends.

Researchers have been investigating mechanisms behind Hofmeister effects for decades.[17-23, 31-36] With respect to interfaces, one hypothesis proposed was that the Hofmeister series at surfaces is due to hydrogen bond ordering of the interfacial water molecules.[18] In this context, kosmotropes are water structure making ions that increase the hydrogen bond ordering of interfacial water molecules and are strongly hydrated. Chaotropes are water structure breaking ions that disrupt the hydrogen bond order of interfacial water molecules and are weakly hydrated.[18] In this thesis, study of SIEs at silica/aqueous interface will be mainly focused on how different ion hydration properties and/or its water structure making or breaking properties would influence the water structure of the silica/water interface.

There have been several studies that have examined specific cation effects at the silica surface. Dove and co-workers performed potentiometric titrations to measure the surface charge density of colloidal silica in the presence of alkali chlorides and alkaline earth chlorides and found that for alkali chlorides, each salt deprotonated the silica surface in the order of $Li^+<Na^+<K^+$.[8] From the results, they suggested that ions such as K^+ that had the most water structure breaking properties promote the most negative charge development.[8] Recently, Brown and co-workers have also shown that the magnitude of the surface charge density of silica increased in the order of $Li^+<Na^+<K^+<Cs^+$.[34] However, they found that the magnitude of the interfacial potential of silica increased in the order of $Cs^+<K^+<Na^+<Li^+$ such that cations that had larger hydration radius had greater magnitude of the interfacial.[34] They reasoned that more hydrated cations were further away from the negatively charged silica surface and had a larger Stern layer thickness, resulting in larger magnitude of the interfacial potential, whereas weakly

hydrated cations were present closer to the surface allowing for more surface deprotonation but a lower in magnitude of the interfacial potential.[34]

In addition, Hofmeister series has been observed to reverse depending on the surface charge density, solution pH and the condition of the surface.[19, 22, 35, 37] Netz and co-workers did molecular dynamics (MD) simulations for halide and alkali ions at both hydrophobic and hydrophilic surface and found that Hofmeister trends could reverse depending on the hydrophobicity of the surface.[35] For a hydrophilic surface, strongly hydrated Li^+ adsorbed to the surface more than weakly hydrated Cs^+. On the other hand, for a hydrophobic surface, the Hofmeister series reversed and Cs^+ adsorbed to the surface more than Li^+.[35] Additionally, Sivan and co-workers used atomic force microscopy (AFM) to show that as ion concentration increased, more cations adsorbed to negatively charged silica and eventually caused overcharging in the d-plane of cations at the electric double layer.[36] However, experimental evidence of the structure of the EDL at the silica/aqueous interface in terms of Hofmeister effects is still not clear and is the subject of our study in Chapter 2.

1.4. Second Harmonic Generation (SHG)

Nonlinear optical techniques such as SHG and SFG can be used to study buried interfaces, which are interfaces that are not exposed to the air such as solid/solid, solid/liquid, and liquid/liquid interfaces. These techniques are surface specific and can also probe an insulating material such as silica.[38-40] In this thesis, non-resonant SHG and resonant-SFG techniques will be used to study silica/aqueous interface. According to the theory, non-resonant SHG technique can be used to study the changes in the interfacial potential under different environmental conditions

such as pH and the type of salts in solution whereas SFG technique can be used to probe specific vibrational transitions of interfacial molecules. The SHG technique will be further discussed in section 1.4 and the SFG technique will be further discussed in section 1.5.

1.4.1. Basic Theory of SHG

Second harmonic generation (SHG) is a non-linear optical technique that is used to specifically probe the surface.

$$\sqrt{I_{2\omega}} \propto E_{2\omega} \propto P_{2\omega}^{(2)} = \chi^{(2)} E_{\omega} E_{\omega} \qquad \text{(Equation 1.1)}$$

In second harmonic generation, two photons of frequency ω shine on the interface spatially and temporally overlapping and induce a second-order polarization ($P_{2\omega}^{(2)}$) resulting in the emission of a small quantity of photons that have twice the frequency of the incident photons.[41] $\chi^{(2)}$ denotes the second order non-linear susceptibility that is intrinsic to the surface and E_{ω} denotes the electric field of incident light from the laser source.[41] The square root of the intensity of second harmonic light generated is proportional to the second harmonic electric field which is proportional to the induced second-order polarization.[41]

The induced polarization, which is equal to the induced dipole moment per unit volume, depends on the strength of the incident electric field. In linear optics, the induced polarization caused by the light is linearly proportional to the incident electric field.[41]

$$P = \varepsilon_0 \chi^{(1)} E \qquad \text{(Equation 1.2)}$$

Where E denotes the applied electric field, ε_0 denotes the vacuum permittivity, $\chi^{(1)}$ denotes the linear susceptibility and P denotes the induced polarization due to E.[41] When the applied electric

field is large enough, it can induce a polarization that responds nonlinearly to the applied electric field.[41]

$$P = \varepsilon_0[\chi^{(1)}E + \chi^{(2)}EE + \chi^{(3)}EEE + ...] \quad \text{(Equation 1.3)}$$

Where $\chi^{(2)}$ denotes the second order non-linear susceptibility and $\chi^{(3)}$ denotes the third-order susceptibility and so on. Under the electric-dipole approximation, $\chi^{(2)}$ and all other even ordered terms are non-zero only in systems that lack inversion symmetry.[41] This allows the SHG technique to be surface-specific. For the fused-silica/aqueous systems where both the silica surface and bulk water are isotropic, it is the break in inversion symmetry arising at the interface of the silica/water that allows for non-zero SHG.[41] Even when a break in symmetry occurs allowing for SHG, nonlinear optical (NLO) responses are typically negligible under low electric field strengths. However, when the electric field is sufficiently intense, such as in the focus of a laser beam, significant NLO signals can be generated.[41] Schematic of SHG at the silica/aqueous interface is shown in Figure 1.2.

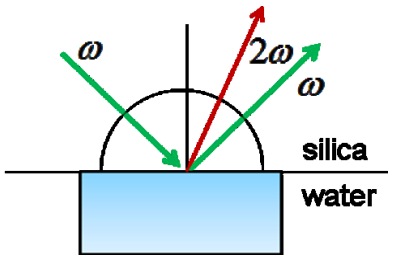

Figure 1.2. Schematic of SHG at the silica/aqueous interface.

As mentioned, $\chi^{(2)}$ is non-linear susceptibility, and it is a unique, intrinsic property of a given surface.[41] $\chi^{(2)}$ can be expressed in terms of the number density of interfacial molecules N and their corresponding molecular hyperpolarizability β.[41] β is the molecular hyperpolarizability that results from intrinsic properties of interfacial molecules. The brackets denote an orientationally averaged value, which gives information on the average molecular orientation at the interface.[41]

$$\chi^{(2)} = N < \beta^{(2)} > \quad \text{(Equation 1.4)}$$

Second-order non-linear susceptibility terms have both resonant and non-resonant terms and can be further expressed as:

$$\chi^{(2)} = \chi^{(2)}_{NR} + \chi^{(2)}_{R} \quad \text{(Equation 1.5)}$$

1.4.2. Reflection and Refraction of Light at Interface

When light interacts with the interface between two media, it can either get absorbed, scattered, refracted or reflected. When the light is entering into a different medium, it will travel at different speed thus, it will bend. The amount it bends depends on the refractive index of two media, and this can be described by Snell's law.[42]

In the case of the silica/water interface, the refractive index for silica is 1.46 and the refractive index for water is 1.33.[43-44] When light is travelling from more dense material (i.e. silica) into less dense material (i.e. water), it will refract as shown in figure 1.3a. As the angle of incidence, $\theta_{i,}$ increases and reaches the critical angle, θ_c, there is only light being reflected and this process is called total internal reflection as shown in figure 1.3b. Total internal reflection is

possible only if the light is travelling from higher refractive index medium to lower refractive index. In our experimental set up, we shine a light at an angle close to the angle of total internal reflection to maximize the reflected light.

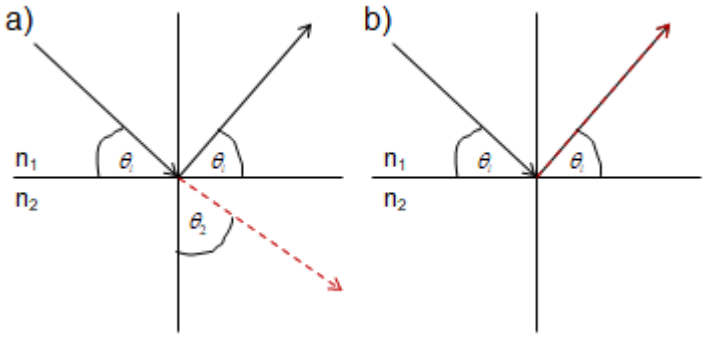

Figure 1.3. Reflection and refraction of light a) when $\theta_i < \theta_c$ b) when $\theta_i > \theta_c$. Refracted light is shown in red (dashed line) and the incident and reflected light are shown in black (bold lines). The refractive index of material 1 (n_1) is greater than material 2 (n_2).

1.4.3. Polarization of Light

Light, also known as electromagnetic radiation, has both an electric and magnetic component and it oscillates in all directions. The polarization of the light component is defined by the direction of oscillation of the electric field.[45] When the electric field is oscillating in random directions, it is called unpolarized.[45] A light bulb and sunlight would be examples of unpolarized light. In linearly polarized light, the electric field is propagating in one direction[45] One of the examples of polarized light is a laser which is used in Sum Frequency Generation (SFG) spectroscopy. Polarized light is used in SFG spectroscopy to get information about the orientation of assembly of molecules at surface. In most SHG and SFG experiments, light is linearly polarized such that it is oscillating either parallel or perpendicular to the plane of

incidence. Plane of incidence is a plane which contains a surface normal. In Figure 1.4., surface normal is defined as z-axis and plane xz is defined as the plane of incidence and y is defined as the axis that is perpendicular to the plane of incidence. When the electric field of light is oscillating along the plane of the incidence, it is called p-polarized light. As shown in Figure 1.4a, electric field of light is oscillating along plane xz. When the electric field of light is oscillating perpendicular to the plane of incident light, it is called s-polarized light. As shown in Figure 1.4b, electric field of light is oscillating perpendicular to plane xz. Dots show the s-polarized light travelling in and out of the page along y-axis. We use different polarization of light for SHG and SFG experiment as each polarization combination is more sensitive to specific $\chi^{(2)}$ tensor elements. By using different polarization combinations, we can get information about the overall orientation of the molecules at the interface.

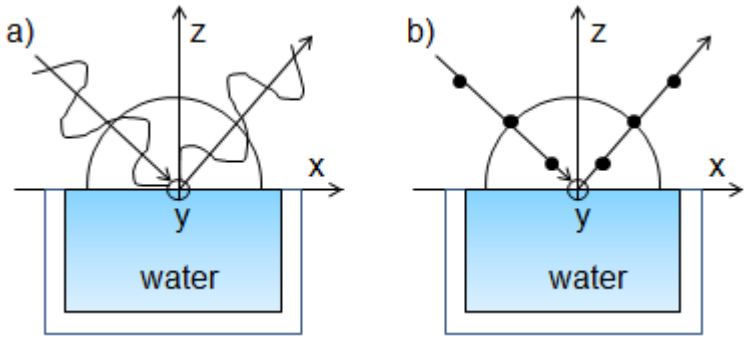

Figure 1.4. a) p-polarized light has its electric field oscillating parallel to the plane of incidence (XZ plane). b) s-polarized light has its electric field oscillating perpendicular to the plane of incidence where the dark black circles denote the electric field oscillating perpendicular to the XZ plane (in and out of page).

1.4.4. Non-resonant SHG

In this thesis, we used non-resonant SHG techniques to look at how different ions affect the interfacial potential of silica. In non-resonant SHG, the frequency of the oscillating electric field present at the interface is not in resonance with the frequency of the incident light.[41] The energy diagram for non-resonant SHG is shown in Figure 1.5. Two photons of frequency ω are absorbed and at the same time, one photon of frequency 2ω is produced.[41] The solid line represents the atomic or molecular ground state, and the dashed line represents the virtual state.[41]

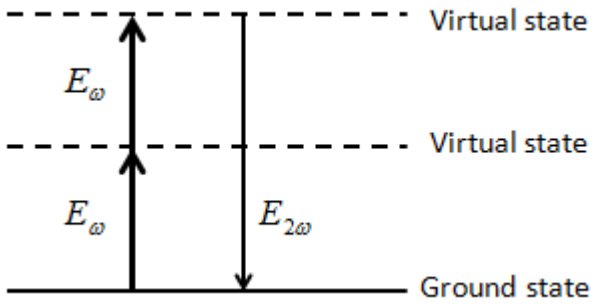

Figure 1.5. Energy diagram for non-resonant SHG.

In 1992, Eisenthal and co-workers showed that a static electric field that is present at a charged silica/aqueous interface can act as another applied electric field and contribute to a $\chi^{(3)}$ term.[46]

$$\sqrt{I_{2\omega}} \propto E_{2\omega} \propto P_{2\omega}^{(2)} = \chi^{(2)} E_\omega E_\omega + \chi^{(3)} E_\omega E_\omega \int E_0 dz \qquad \text{(Equation 1.6)}$$

The integration of the static electric field, E_0, from the surface extending into the bulk will give an interfacial potential term, Φ_0, that contributes to $\chi^{(3)}$.[46]

$$\sqrt{I_{2\omega}} \propto P_{2\omega}^{(2)} = \chi^{(2)} E_\omega E_\omega + \chi^{(3)} E_\omega E_\omega \Phi_0 \qquad \text{(Equation 1.7)}$$

Second order non-linear susceptibility terms have both resonant and non-resonant terms. Using non-resonant SHG, it will only probe non-resonant second-order susceptibility, $\chi_{NR}^{(2)}$ that includes water, silica, and ions present at the interface.[47]

$$\chi_{NR}^{(2)} = \chi_{H2O}^{(2)} + \chi_{silica}^{(2)} + \chi_{ions}^{(2)} \qquad \text{(Equation 1.8)}$$

Eisenthal and co-workers have assumed that changes in the $\chi^{(2)}$ term are small and any changes in the SHG intensity as a function of pH are mainly due to the $\chi^{(3)}$ term.[46] For instance, as the silica surface gets more deprotonated, it becomes more negative and causes more alignment of water molecules at the interface. This increases the magnitude of Φ_0, which increases $I_{2\omega}$.

The $\chi^{(3)}\Phi_0$ term from equation 1.7 can be further expanded to:

$$\chi^{(3)}\Phi_0 = N_{H_2O}\left(\frac{\mu_{H_2O}\Phi}{bkT}\right)\beta_{H_2O} + N_{H_2O}\gamma_{H_2O}\Phi\,. \qquad \text{(Equation 1.9)}$$

Where N_{H_2O} is number density of water molecules at the interface, μ_{H_2O} is a transition dipole moment of water molecules, β_{H_2O} denotes the molecular hyperpolarizability of water, b is a constant, k is the Boltzman constant, T is temperature, and Φ denotes the interfacial potential.[46] The first term describes the amount of water molecules aligned due to the interfacial potential. γ_{H_2O} is a second-order molecular hyperpolarizability of water, and it is assumed to be small leading to negligible contribution from the second term. Based on the above equation, the pH-dependence of the SHG signal stems from the amount of ordered water molecules at the interface that changes as the interfacial potential is changed. Figure 1.6 shows an example of the non-resonant SHG at the silica/aqueous interface for 0.1 M NaCl solution from pH 7-2 where the

intensity of SHG was plotted as a function of pH. As pH increases, the intensity of SHG increases as the silica surface becomes more negative and there is more aligned water molecules at the silica/aqueous interface. However, our group's recent research showed that the changes in the SHG intensity may not only be caused by the $\chi^{(3)}\Phi_0$ term, but also by the $\chi^{(2)}_{silica}$ ($\chi^{(2)}$ of silanol groups, $\chi^{(2)}$ of siloxide groups).[48]

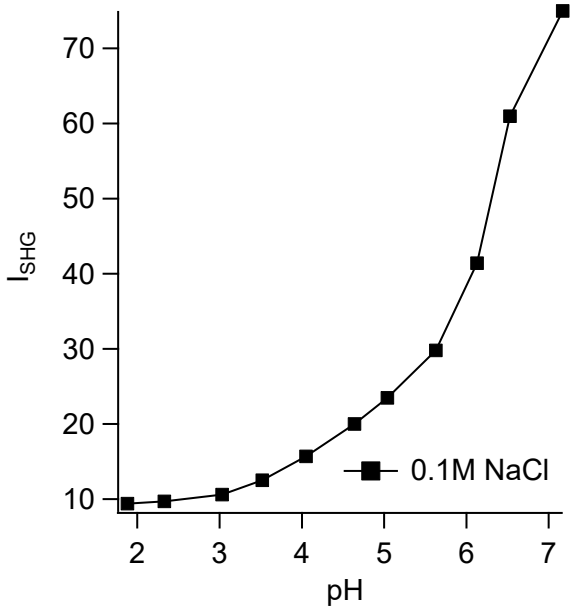

Figure 1.6. Example of SHG at the silica/aqueous interface from pH 7-2.

1.4.5. Studies on the Specific Ion Effects at Silica/Aqueous Interface using SHG

Under the constant capacitance model, the electric field of SHG, proportional to the interfacial potential, can be related simply to the amount of deprotonation of the surface as the surface charge density of silica is directly proportional to the interfacial potential under high salt concentration (≥ 0.1 M) where this model is typically implemented.[46] Our group adopted this model first employed by the Eisenthal group to study the silica/aqueous interface in the presence of high salt concentration and showed that the acid-base chemistry of silica is affected by the

presence of specific ions in the solution using the SHG technique.[38-40, 49] For example, Azam et al has shown that the effective acid dissociation constant, Ka_{eff}, increased in the order of $Na^+ > Li^+ > K^+ > Cs^+$ attributed to different solvation environments of the silanol groups in the presence of the different ions.[38]

In this thesis, we will also be using SHG techniques under high salt concentration and investigate how the silica surface charge changes under the presence of specific ions such as bicarbonate and chloride ions in Chapter 3.

1.5. Sum Frequency Generation (SFG)

Resonant enhanced SFG allows us to specifically probe interfacial molecules of our interest. In the case of the silica/aqueous interface, we can use SFG to probe interfacial water molecules at the silica/aqueous interface. Non-resonant contributions from water and the silica surface may also contribute.[47] Nonetheless, the interfacial water molecules that exhibit resonant vibrational frequency of OH will be the dominant factor that causes the SFG signals.

1.5.1. Basic Theory of SFG

Sum frequency generation (SFG) is a non-linear optical technique where one photon of visible and another photon of IR photons will hit the surface with spatial and temporal overlap to generate photons that have the frequency at the sum of the visible and IR frequency. The equation describing SFG is similar to the equation that describes SHG. The square root of the intensity of the sum frequency generated is proportional to the induced polarization oscillating at the sum frequency.

$$\sqrt{I_{SFG}} \propto E_{SFG}^{(2)} \propto P_{SFG}^{(2)} = \chi^{(2)} E_{VIS} E_{IR} + \chi^{(3)} E_{VIS} E_{IR} \int E_0 dz \quad \text{(Equation 1.10)}$$

$$\sqrt{I_{SFG}} \propto E_{SFG}^{(2)} \propto P_{SFG}^{(2)} = \chi^{(2)} E_{VIS} E_{IR} + \chi^{(3)} E_{VIS} E_{IR} \Phi_0 \quad \text{(Equation 1.11)}$$

$$\chi^{(3)} \Phi_0 = N_{H_2O} \left(\frac{\mu_{H_2O} \Phi}{bkT} \right) \beta_{H_2O} + N_{H_2O} \gamma_{H_2O} \Phi \quad \text{(Equation 1.12)}$$

$$\chi^{(2)} = \chi_{NR}^{(2)} + \chi_R^{(2)} \approx \chi_R^{(2)} \quad \text{(Equation 1.13)}$$

$$\chi_R^{(2)} = N_{H_2O} < \beta_{H_2O} > \quad \text{(Equation 1.14)}$$

Figure 1.7 shows SFG at the silica/aqueous interface and the corresponding energy diagram. Similar to SHG, sum frequency signals are also only expected when there is a break in inversion symmetry (based on the electric dipole approximation). Moreover, SFG is enhanced only if the interfacial molecules exhibit vibrational transition that match with the wavelength of the incident IR light and if the vibrational mode is both IR and Raman active. This allows us to examine particular vibrational stretches such as OH stretches in water. Specifically, at the silica/aqueous interface, we shine a beam of IR light from 3000 to 3600 nm to probe OH stretches at the interface, which will come from the interfacial water molecules. Figure 1.8 shows an example of the SFG spectra of silica/water interface at pH of 5.6. Between the wavenumber of incident IR from 3000 to 3600 nm, we observe one dominant peak appearing at ~3200 cm^{-1} and one small peak appearing at ~3400 cm^{-1}, which will be discussed more in Chapter 2. Since the vibrational transition frequency of water matches with the frequency of the incident IR electric field of light, the intensity of SFG would be mainly caused by the contribution from $\chi^{(2)}$ or $\chi^{(3)}$ of interfacial water molecules. Thus, we can specifically probe interfacial water molecules at silica/aqueous interface using the resonant SFG technique.

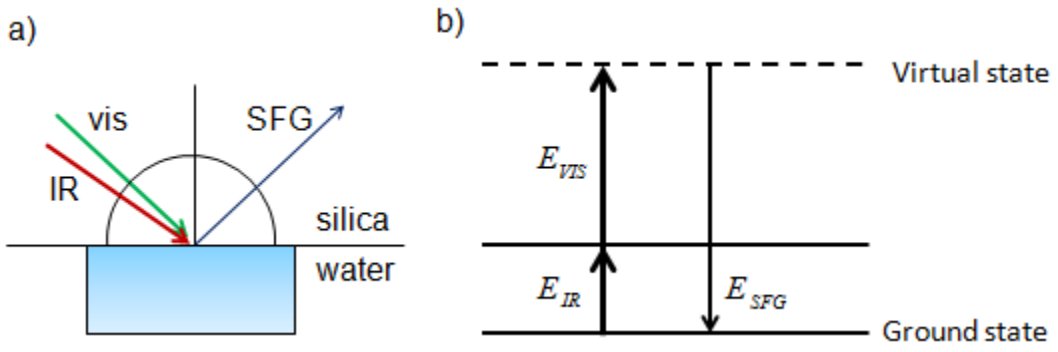

Figure 1.7. a) SFG at the silica/water interface and b) energy diagram of resonant SFG.

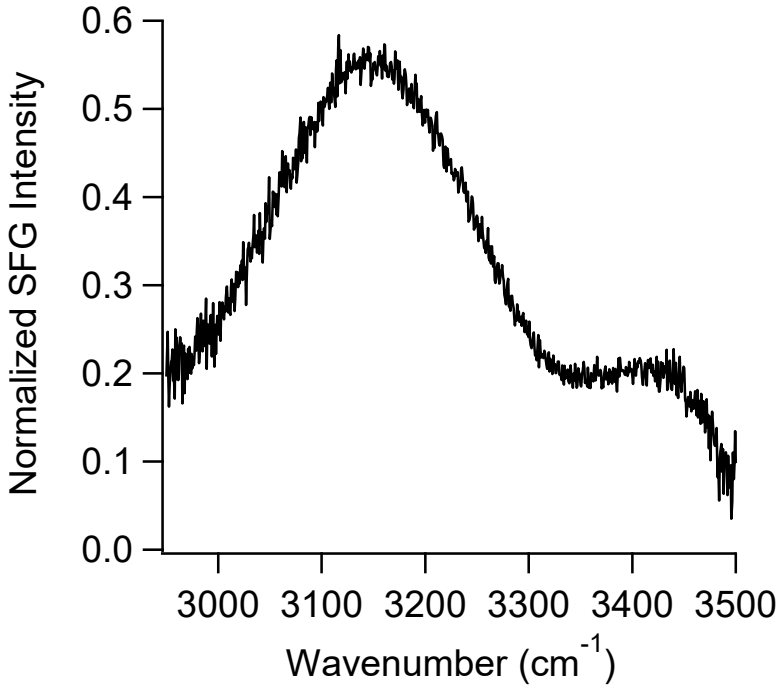

Figure 1.8. Example of an SFG spectrum of water (pH~ 5.6) at the silica/water interface.

1.5.2. Second order Non-linear Susceptibility in Resonant SFG

$\chi^{(2)}$ is a rank 3 tensor containing 27 tensor elements. In Cartesian coordinate system, $\chi^{(2)}$ can be written as $\chi^{(2)}_{IJK}$, where I denotes the direction of the vector component of the SFG

electric field, *J* denotes the direction of the vector component of the incident visible electric field, and *K* denotes the direction of the vector component of the incident IR electric field. For example, $\chi^{(2)}_{XZZ}$ would be the tensor element that probes the x-component of the SFG electric field, and z-component of the visible and IR electric field. The magnitude of $\chi^{(2)}_{XZZ}$ tensor would give information about how much x-polarized SFG is generated when z-polarized visible and z-polarized IR electric fields are applied. Depending on the properties of the interface, sum frequency may be generated more in one polarization combination than another, as a result of certain tensor elements being larger in magnitude. Additionally, the presence of symmetry in the system probed by SFG may result in equalities between the individual elements as well as some zero-valued tensor elements. For example, the silica aqueous interface has $C_{\infty v}$ symmetry. We can perform all possible symmetry operations on interfaces that have $C_{\infty v}$ symmetry, and we will end up having 4 non-zero, unique tensor elements:

$$\chi^{(2)}_{ZZZ}, \chi^{(2)}_{XXZ} = \chi^{(2)}_{YYZ}, \chi^{(2)}_{ZXX} = \chi^{(2)}_{ZYY}, \chi^{(2)}_{YZY} = \chi^{(2)}_{XZX}$$

Polarized light is used to probe specific tensor elements of the silica/aqueous interface. As shown in Figure 1.9, at the silica/aqueous interface, we set the plane of incidence to be XZ plane. In this case, p-polarized light would then be the electric field of light that is oscillating parallel to XZ plane and s-polarized light would be the electric field of light that is oscillating perpendicular to XZ plane. Thus, different combinations of polarized of light can probe different tensor elements. For example, for ssp-polarized light (s-polarized SHG, s-polarized visible, p-polarized IR), it can probe the $\chi^{(2)}_{YYZ}$ tensor element. By probing different tensor elements, the information on the orientation of the molecule of interest can be obtained.

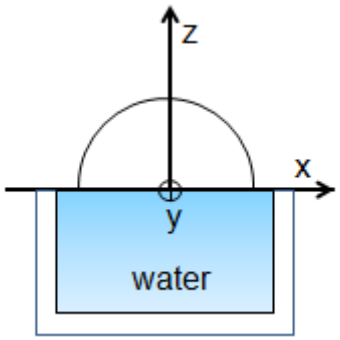

Figure 1.9. Silica/water interface with a defined laboratory coordinate frame x,y,z. Plane of incidence is XZ plane.

1.5.3. Scanning and Broadband SFG

SFG spectroscopy can be performed by two different experimental methods: scanning and broadband SFG. In scanning SFG, visible light and IR light are narrow in frequency (<10 cm^{-1}). IR light is tuned and scanned point by point over a wide range of wavenumbers while visible light remains the same. In broadband SFG, visible light is narrow in frequency (<10 cm^{-1}) and IR light is broad in frequency. For example, the full width half maximum (FWHM) of our IR pulse is ~120 cm^{-1}. Scanning SFG acquires data point by point, so it is easier to use but often takes long time to acquire data. Broadband SFG can collect a larger portion of the spectrum at once, so it takes less time to collect data. However, it requires a femtosecond IR pulse rather than a picosecond pulse. In this thesis, the OH vibrational stretching region was observed to look at interfacial water molecules at the silica/aqueous interface, and six broadband IR pulses centered at different frequencies were collected and summed up for further data analysis. To obtain SFG spectrum of water, since the water spectrum is very broad, six IR pulses were acquired at six different central frequency of the IR band.

1.5.4. Studies on Specific Ion Effects at the Silica Interface using SFG

Previously, SFG have been used to study how ion identity affects the water structure at the silica/aqueous interface.[32-33, 50-51] Hore and co-workers have used SFG spectroscopy to examine the effect of NaCl concentration on the SFG water spectrum of the silica/aqueous interface, and saw that the SFG signal decrease as salt concentration increased.[52] From the SFG results, they could infer how much the interfacial water structure was perturbed by looking at how much of the SFG signal has decreased. Chou and co-workers measured the SFG spectra of different monovalent alkali chloride solution at silica/aqueous interface. They saw that as salt concentration increases, the SFG signal also decreases due to cation charge screening the surface.[51] They also found that the degree of perturbations of interfacial water structure at silica/aqueous interfaced followed the order of $K^+ > Li^+ > Na^+$.[51] However, Cremer and co-workers studied the effect of monovalent, divalent and polyatomic ions at silica/aqueous interface at pH 10 and found that the degree of perturbation followed the following order which followed direct Hofmeister series: $Li^+ > Cs^+ > K^+ > Na^+$.[33] These results suggest that specific ion effects were observed at silica/aqueous interface and it also suggests that these specific ion effects might be dependent on both the pH and concentration of the solution.

Since these SFG studies were all measured either at different ion concentrations and/or at different pH values. Therefore, it is hard to draw a conclusion regarding how each ion influences the interfacial water structure at the silica/aqueous interface based on these studies alone. In this thesis, vibrational SFG spectroscopy is used to probe water structure at the aqueous/silica interface in the presence of four different 0.5 M monovalent alkali chlorides condition over a wide range pH (pH 2-12) to investigate specific ion effects under varied pH conditions.

1.6. Thesis Organization

The silica/aqueous interface is important in many geological and environmental applications as silica is abundant on earth and it is, therefore, of great interest to determine the molecular interactions that are present at silica/aqueous interface under different environmental conditions such as composition of salt, concentration of salt, and pH. In this thesis, specific ion effects at the silica/aqueous interface will be investigated using second harmonic generation (SHG) and sum frequency generation technique.

Chapter 2 describes the effects of 0.5 M monovalent cations on the interfacial water structure at the silica/aqueous interface and looks at how different ion size and hydration shell could influence the ordering of interfacial water molecules and the acid-base behavior at the silica/aqueous interface. Sum frequency generation (SFG) spectroscopy was used to probe the relative ordering of interfacial water molecules at the silica/aqueous interface by probing the OH vibrational stretching region. Our results suggest that each different ion had different adsorption behavior and also changed the ordering of interfacial water differently. Moreover, we observe that these specific ion effects (SIE) vary as a function of pH, and we observe reversal of the Hofmeister series at high pH. In addition, we were able to probe two different populations of water at the surface, those close to the surface in the Stern layer and those in the diffuse layer, and observe different SIEs for the two different water populations.

Chapter 3 describes the effects of bicarbonate ions on the silica/aqueous interface near neutral pH. Once again, sum frequency generation (SFG) was used to probe the OH vibrational stretching region at the silica/aqueous interface for 0.1 M sodium bicarbonate and 0.1 M sodium chloride solution and the results were compared. Next, SHG techniques were used to investigate

the adsorption behavior of bicarbonate ion at the silica/aqueous interface and resulting changes in the acid-base chemistry of silica. The ssp and pss polarization combinations were used for both SHG and SFG measurements. Our results show that bicarbonate partitions towards the Stern layer and reduces the screening of the Na^+ cations. In addition, both SFG and SHG results suggests that there is hysteresis; in other words the history of the starting pH of the solution in the titration experiments influenced the resulting SHG indicating we were not observing the thermodynamic minimum of the surface, but rather kinetically trapped structures.

Chapter 4 describes the conclusion of this thesis and future work.

Chapter 2

pH-dependent inversion of Hofmeister trends in the water structure of the electrical double layer

Portions of this chapter are reproduced with permission from Dr. Kerian and Dr. Gibbs

DeWalt-Kerian, E. L.; Kim, S.; Azam, M. S.; Zeng, H.; Liu, Q.; Gibbs, J. M., pH-Dependent Inversion of Hofmeister Trends in the Water Structure of the Electrical Double Layer. *J. Phys. Chem. Lett.* **2017**, 2855-2861.

Experiments related to the specific cation effects were done in collaboration with Dr. Kerian and the final manuscript composition was written by Dr. Kerian and Dr. Gibbs.

2.1. Introduction

The chemistry of water at the mineral/water interface is complex and remains a source of some debate. The complexity of the silica/water interface is largely due to deviations in the behavior of water molecules at the interface from their counterparts in the bulk liquid. In addition, water molecules at the surface can exhibit vastly different properties depending on the nature of the interface. For instance, the hydrogen-bonding structure of interfacial water is substantially different from that of bulk water when in contact with a charged solid surface[1, 53-55] or even when in the proximity of apparently an inert surface, such as a simple metal.[23, 31-32, 56-58] The solution pH and electrolyte composition are among the most important parameters that affect the behavior of water at the silica/water interface. Many studies have examined the effect of pH on dissolution rates of silica and quartz.[2, 7, 59-66] In addition, it has been found that alkaline and alkaline earth cations dramatically increase the rate of dissolution of silica and quartz,[67-70] with possible mechanisms of dissolution related to cation hydration and imposed changes in water orientation at the silica/aqueous interface.[71-72] Consequently, elucidating the structural properties of water at the silica/water interface is crucial in understanding the interfacial phenomena that play significant roles in chemical separations, geochemical, petrochemical, environmental and biological processes, which are all greatly influenced by the abundance, molecular structure and orientation of the water molecules at the interface.[2, 38, 46, 51, 73-86]

In order to understand the effect of ions on the molecular structure of the water molecules at the charged silica/water interface, double-layer models are often used, with the Gouy-Chapman-Stern-Grahame (GCSG) model generally accepted as the most relevant model in the case of silica/water in electrolyte solutions of relatively high ionic strength.[15, 87-89] According to the GCSG model, water molecules that lie between the negatively charged silica surface (0-plane)

and the first layer of hydrated cations non-specifically adsorbed at the outer Helmholtz plane (OHP) make up the compact region of the electrical double layer (EDL), also known as the Stern layer. Excess cations in the diffuse layer further screen the negative surface charge of the silica until electroneutrality is reached. From a simple electrostatic model of water alignment, the potential at the OHP (Φ_{OH}), which is approximately equal to the experimentally observable zeta potential, aligns water molecules in the diffuse layer. As cations are added, charge screening occurs resulting in a smaller Φ_{OH} and less aligned water.[90] A simplified depiction of the GCSG model is shown in Figure 2.1. The Φ_{OH} aligns water molecules in the diffuse layer, and the effect of cation charge screening can be observed by the corresponding decrease in water alignment. In pure water, the isoelectric point (IEP) of silica (where $\Phi_{OH} = 0$) is the same as its point of zero charge (PZC) which is at pH~ 2-3. However, the presence of cations and resulting charge screening can shift the IEP to higher pH. The affinity for adsorption at the surface can differ among ions, leading to IEPs that are dependent on the ionic species present in solution. Accordingly, much emphasis has been placed on understanding specific ion effects (SIE) on Φ_{OH} and water ordering at the silica/water interface for cations. SIEs are often interpreted in the context of their position within the Hofmeister series, which arranges the ions in order from their ability to salt-in proteins. This series directly corresponds to ion size and hydration. Arranged by ionic radii, the Hofmeister series for the alkali cations is $Li^+ < Na^+ < K^+ < Cs^+$ or when arranged by hydration is $Cs^+ < K^+ < Na^+ < Li^+$. This Hofmeister series can also rank ions according to their ability to disrupt or strengthen hydrogen bonding in bulk water, with poorly hydrated Cs^+ and K^+ being characterized as chaotropes ("structure breakers") and the small, strongly hydrated ions Na^+ and Li^+ being characterized as kosmotropes ("structure makers"). A wide variety of

tools and methodologies have been used to investigate SIEs at the silica/water interface, and to understand these effects within the context of the Hofmeister series.[2, 32 , 38, 50-51, 71]

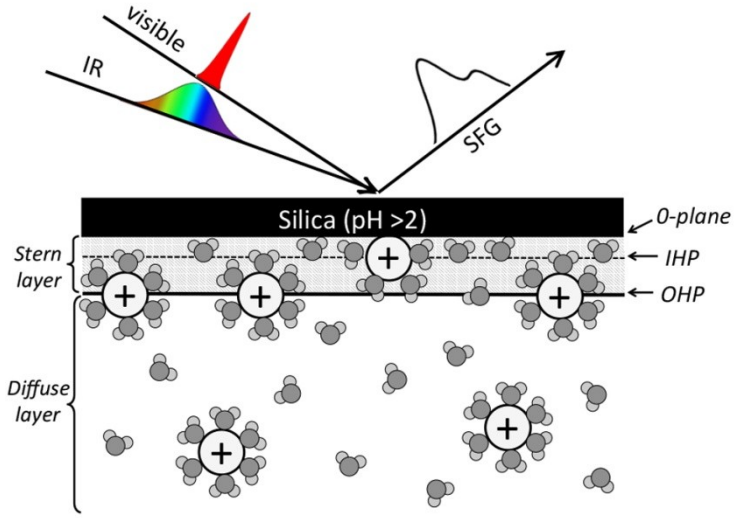

Figure 2.1. An overview of the GCSG model of the EDL at a charged silica/water interface in the presence of monovalent cations. The process of broadband SFG is also shown, where a broadband IR pulse is overlapped with a narrowband visible pulse at the silica/water interface to generate the SFG water spectrum.

Nonlinear optical methods including second harmonic generation (SHG) and sum frequency generation (SFG) have proven to be powerful methods for probing the silica/water interface, and offer key advantages over other analytical methods. Due to the unique and intrinsic selectivity of second order nonlinear optical processes for noncentrosymmetry, in SHG and SFG methods signal is only generated where there is a break in symmetry. Such a break in symmetry arises in ordered systems, such as certain types of crystals, and interfaces, with no signal being generated from isotropic solutions or amorphous solids.[1, 46, 91] In particular, vibrational SFG has been used extensively in the study of molecular structure of water at interfaces.[1, 46, 83, 92-95] By

tuning the IR light source, the vibrational modes of water can be selectively probed such that water is the only molecular species measured. An increase of water order in the system causes a corresponding increase in SFG signal. In the case of pH-dependent measurements of silica, changes in the Φ_{OH} that affect the ordering of water in the diffuse layer can be probed with vibrational SFG measurements (known as the $\chi^{(3)}$ technique).[96-98] For the experiments presented in this work, broadband SFG is used where we have a broad (FWHM ~ 120 cm^{-1}) IR pulse and a narrowband (FWHM ~ 10 cm^{-1}) visible pulse temporally and spatially overlapped (Figure 2.1).

Vibrational SFG has been used to examine the effect of changes in pH and electrolyte composition on the interfacial hydrogen-bonding network of water at the silica/water interface. [1, 92-93, 99] SIEs on the SFG spectrum of water at silica/water interface were first reported by Yang et al, where perturbation of the water structure at the interface was monitored upon adding Li^+, Na^+ and K^+ up to 0.1 M concentration at pH ~ 5.7.[51] The authors observed the greatest SIEs at low concentrations (0.5 mM), with K^+ disrupting the water structure the most and Na^+ the least, indicating adsorption in the following order $K^+ > Li^+ > Na^+$.[51] In a follow up study, Lovering et al confirmed that at pH ~6, Li^+ led to more disruption in water structure than Na^+ at high concentrations (6 M).[97] However, an opposite trend was observed in a study by Flores et al. In this work, SIEs were examined using SFG for the quartz/water interface at pH 10 in the presence of low concentrations of different monovalent and divalent cations (≤ 1 mM).[33] For monovalent cations, they found that the alkali metal ions attenuated the water structure at the interface following a direct Hofmeister series, with the exception of Li^+, which led to the least attenuation indicating adsorption in the following order: $Na^+ > K^+ > Rb^+ > Cs^+ > Li^+$.[33] The differences in the SIEs observed in these studies may be attributed to differences in electrolyte concentrations and pH. Nonetheless, a systematic examination of SIEs of monovalent cations at the silica/water

interface over a wide pH range and constant electrolyte concentration has yet to be performed using SFG spectroscopy.

It is generally reported that cation adsorption on negatively charged silica follows a direct Hofmeister series: $Li^+ < Na^+ < K^+ < Cs^+$,[100-102] which is inversely related to hydrated cation radius. In addition, most models of the mineral oxide/aqueous interface contain a capacitance parameter that is directly related to the distance of ions from the surface (ie. the distance of the OHP from the surface)[103] and has been found to correspond to hydrated ionic radius.[9, 103] The majority of capacitance values are reported for a single pH and when used to interpret potentiometric measurements are assumed to be pH independent. However, there is some experimental evidence to suggest that the ordering of cation adsorption is pH dependent. Specifically, an AFM study by Morag et al identified pH-dependent changes in cation adsorption on silica at 10 mM electrolyte concentrations. They found that Cs^+ adsorbs strongly to the silica surface at pH < 7, with adsorption increasing as a result of increasing ion concentration. It was observed that at low pH (< 7), the monovalent cations adsorbed the most strongly following a direct Hofmeister series $Li^+ < Na^+ < K^+ < Cs^+$.[19] Strikingly, an inversion in this series was observed at high pH (pH >7), with small, strongly hydrated ions binding more strongly to the surface in the following order: $Cs^+ < K^+ < Na^+ < Li^+$ [9, 19, 104-105]. These findings corroborated early evidence of a reversal in cation adsorption affinity for silica colloids at pH > 7 by Tadros and Lyklema.[106] These studies have also been substantiated by molecular dynamics (MD) simulations, where Li^+ and Na^+ have been found to be more strongly adsorbed to silica than Cs^+ at large negative surface charge densities, which is the opposite of the direct Hofmeister order observed at neutral and low pH.[98, 107]Although these experimental studies have provided insight on cation adsorption, they are centered on macroscopic measurements and offer limited

understanding on changes in the molecular structure of water within the EDL. Performing SFG measurements over a wide pH range should be able to offer insight on water structure at the molecular level for different electrolytes, and offer insight on previous SFG studies that were performed for a single pH point. In this work, SFG measurements of the silica/water interface were acquired over a broad pH range (2-12) for 0.5 M LiCl, NaCl, KCl and CsCl, revealing SIEs on water structure are highly pH dependent. This relatively high salt concentration was chosen for its relevance to the GCSG model, as both the Stern layer and diffuse layer should be present.

2.2. Experimental

2.2.1. SFG Instrumentation

The laser system used in this study has been described previously.[38-40] Briefly, the system consists of a regeneratively amplified laser (Spitfire Pro, Spectra Physics, 1 kHz, 100 fs, 3.5 W) that is seeded and pumped by a femtosecond Ti:Sapphire oscillator (Spectra Physics, Mai Tai, 80 MHz) and a Nd:YLF laser (Spectra Physics, Empower), respectively. Two-thirds of the output light of this Spitfire (2.3 W) was used to pump a TOPAS-C optical parametric amplifier (Light Conversion). The resulting broadband infrared light (FWHM ~130 nm) was tuned by using a non-collinear difference frequency generator (NDFG) in the range of 2750 – 3300 nm to probe the broad O-H stretching modes of the interfacial water molecules. Visible light from the Spitfire (100 fs, λ = 800 nm) was stretched to a ps pulse using a Fabry-Perot etalon (FWHM ~ 10 cm^{-1}) to generate a narrowband pulse (FWHM < 1 nm). The p-polarized fs IR light (~20-25 μJ/pulse) and the s-polarized ps visible light (~10 μJ /pulse) were focused onto the fused silica/water interface at angles of 64° and 60°, respectively, from surface normal. These two fields were then

spatially and temporally overlapped on the silica/aqueous interface to generate the sum frequency light. SFG light from the sample was recollimated and filtered with a bandpass filter to remove the residual 800-nm light (Chroma, HQ 617/70 M) and passed through a polarizer to select s-polarized SFG. The filtered and polarized SFG was then focused onto a spectrograph (Acton SP-2556 Imaging Spectrograph, grating: 1200 G/mm with 500-nm blaze wavelength), which was coupled with a thermoelectrically cooled (-75 °C), back-illuminated, charge coupled device camera (Acton PIXIS 100B CCD digital camera system, 1340 x 100 pixels, 20 μm x 20 μm pixel size, Princeton Instruments).

2.2.2. Preparation of Silica Surface

The IR grade silica hemispheres were obtained from Almaz Optics, NJ, USA. Prior to use, the hemisphere was cleaned by sonicating it in Milli-Q water (5 min), then in methanol (5 min) and finally in water (5 min) again, with copious rinses of Milli-Q water in between sonications. The hemisphere was then immerged in Piranha solution (3:1 mixture of H_2SO_4 and 30% H_2O_2, for an hour followed by a thorough washing with Milli-Q water. The hemisphere was then sonicated in water for 5 minutes for a total of three times, with rinses of Milli-Q water in between sonications. The cleaned hemisphere was kept in the Millipore water until it was used for SFG experiments. Another hemisphere was cleaned in the same way as described above and coated with gold (thickness of 200 nm) through chemical vapor deposition to provide a standard for data normalization.

2.2.3. Preparation of Salt Solutions

Salt solutions (0.5 M) were prepared by dissolving salts in ultrapure deionized water (18.2 MΩ·cm, MilliQ-Plus ultrapure water purification system, Millipore). All the solutions were

prepared by using the inorganic salts as obtained and without any further purification. The pH of the solutions were adjusted using the corresponding base (hydroxide of same alkali metal ions) or acid (same hydrochloric acid) solutions. The pH of all the solutions were measured with an Orion Versa Star, Star A, and Dual Star meters from Thermo Scientific (Orion, 8157UWMMD).

2.2.4. Materials

High purity salts, acids and bases were selected for preparation of the salt solutions NaCl (≥99.99%, Fisher Scientific), NaOH (≥ 99.99%, Sigma-Aldrich) KCl (≥99.999%, Fisher Chemical), KOH (≥99.98%, Fisher Chemical), LiCl (≥99.99%, Sigma-Aldrich) , LiOH (≥98%, Sigma-Aldrich), CsC; (≥99.99%, Fisher Chemical), CsOH (≥99.9%, Fisher Chemical) and HCl (trace metal grade, Fisher Scientific) were used. Sulfuric acid (95.0-98.0%, Caledon Laboratories) and hydrogen peroxide were purchased from Sigma-Aldrich for Piranha cleaning. All materials were used without further purification. Ultrapure deionized water (18.2 MΩ) was used after deionization from a Milli-Q-Plus ultrapure water purification system (Millipore). All experiments were performed with freshly prepared solutions.

2.2.5. SFG Experiments

Prior to start of each experiment, six reference SFG spectra were collected from a gold-coated IR grade silica surface covering the infrared region from 3000 to 3500 cm^{-1}, which includes the majority of OH-stretching region of the water spectrum. The SFG spectra were adjusted by varying the incident IR wavelength so that the IR was centered at ~3000, 3100, 3200, 3300, 3400 and 3500 cm^{-1}. The polarization combination ssp (s-SFG, s-vis and p-IR) was used, which is commonly used to monitor the structure of water at the interface.[46, 51-52, 54, 58, 83, 93-95, 108] The gold-coated hemisphere was then replaced with a bare IR grade silica hemisphere and

aligned using irises to make sure the reflected beam from the silica/water interface maintained the same alignment as the beam reflected from the gold surface. Similarly, six spectra at the same central wavenumbers were measured for the silica/water interface. The six spectra from the silica/water interface were then summed to generate a single spectrum covering the broad water spectrum. The summed water spectrum was then normalized by dividing by the sum of the six gold reference spectra and finally smoothed to obtain the gold-normalized spectrum of interfacial water.[39-40] A freshly cleaned fused silica hemisphere (Almaz optics, 1 inch diameter, IR-grade SiO_2) was used for each SFG experiments. The hemisphere was placed on a custom-built Teflon cell so that the flat surface of the hemisphere was in contact with the aqueous phase. The silica/water interface was perpendicular to the surface of the laser table, and the aqueous phase was exposed so the pH could be routinely monitored and changed by adding solution from the top. Experiments for either a low pH or a high pH solution was performed for one cleaned hemisphere. First, SFG was measured for the silica/water interface with the Milli-Q water that has been equilibrated with air (~pH 5.6). The Milli-Q water was then replaced with ~10mL of the salt solution without pH adjustment (pH between 5-6 depending on the salt) and the interface was equilibrated for 30 min. After the equilibration time, a full spectrum was acquired. Aliquots of the corresponding acid or base solution with the same salt concentration (0.5 M) were added to adjust the pH by ~1 pH unit without altering salt concentration. After the addition of each aliquot, the solution was mixed by repeatedly removing and redispensing the solution with a glass pipet fit with a rubber bulb. At each new pH, the system was allowed to stand for ~3 min to reach equilibrium before the SFG spectrum was collected. For the high pH experiments, pH was adjusted in intervals of one pH unit until pH of the solution reached ~12.0. For the low pH experiments, pH was adjusted until pH of the solution reached ~ 2.0. Each experiment was

performed a minimum of three times.

2.3. Results and Discussion

2.3.1. SFG Results

In this work, vibrational SFG spectroscopy was used to monitor SIEs on water structure at the silica/water interface. Four electrolytes were studied: LiCl, NaCl, KCl and CsCl. Since the focus of this work is on cation specific effects, the counter anion, Cl^-, was kept the same for all experiments. Under the experimental configuration as described in the experimental section, two main peaks were typically observed in the OH stretching region of the ssp SFG water spectrum: one centered at ~3200 cm^{-1} and one at 3400 cm^{-1}, which is consistent with previously reported SFG water spectra.[51, 95-96, 99] After acquisition of the water spectrum, the pure water was replaced with one of the four 0.5 M electrolyte solutions and another spectrum was acquired. The pH was then decreased from its starting pH of ~6 until a bulk pH 2 was reached or increased until pH 12 was reached. The ssp SFG spectra of water were smoothed by taking the moving averaging of every 3 data points, and only ever 3rd data point is displayed. Smoothed ssp SFG spectra water in the presence of the 0.5 M electrolytes from pH 2 – 12 are shown in Figure 2.2.

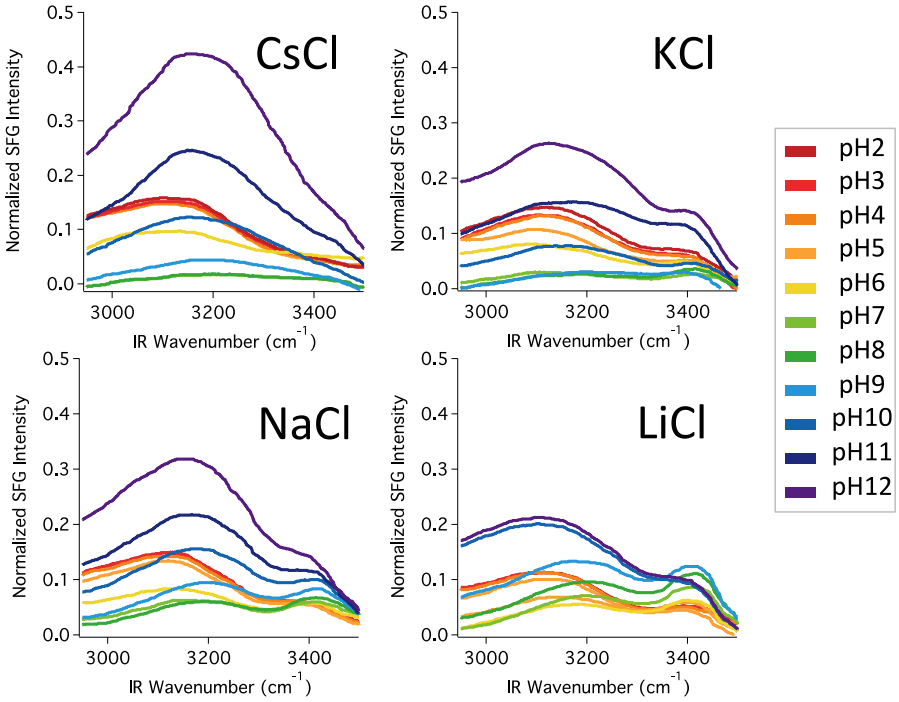

Figure 2.2. Smoothed ssp SFG spectra of water in the presence of 0.5 M CsCl, KCl, NaCl and LiCl at pH values from 2-12.

Several trends can be qualitatively observed in the spectra shown in Figure 2.2. Although the spectral shape varies somewhat between the different experiments, one consistent feature in all of the spectra is the dominant 3200 cm^{-1} peak and smaller 3400 cm^{-1} peak. These two peaks appear to exhibit different pH-dependent behaviors, but are difficult to determine by simple visualization of the spectra and will be addressed in detail in following paragraphs. It is clear that at pH > 10, CsCl has the highest SFG intensity out of the four salts, but at neutral pH has the lowest intensity. For LiCl, the intensity of the water spectrum appears to plateau at pH 11, but for the other three salts SFG intensity continues to increase up to pH 12. Though these trends are somewhat obvious from visual inspection of the spectra in Figure 2.2, a more concise and quantitative method is needed to clearly identify different pH dependent trends among the four

salts. Therefore, integration of the spectra was performed to quantify overall trends in spectral intensity. By integrating the water spectra, mean SFG intensity (which is related to net water order) as a function of pH can be determined for the different cations. Each pH titration was performed a minimum of three times and the ssp water spectrum for each trial was integrated over the range of 2950-3450 cm^{-1}. The mean integrated intensities for each salt are shown in Figure 2.3. This integration range was chosen as it contained the bulk of the water spectrum where the signal-to-noise ratio (S/N) was sufficient for integration. Although such analysis reduces the information content of the spectrum to a single scalar value, it offers key advantages over peak-fitting including simplicity, robustness and avoidance of overfitting and user bias. While the integrated plots do not offer insight on the relative behavior of the 3200 cm^{-1} and 3400 cm^{-1} peaks within the spectrum, they are able to provide a general indication of the differences in the amount of disruption of the water structure at the interface between the four electrolytes.

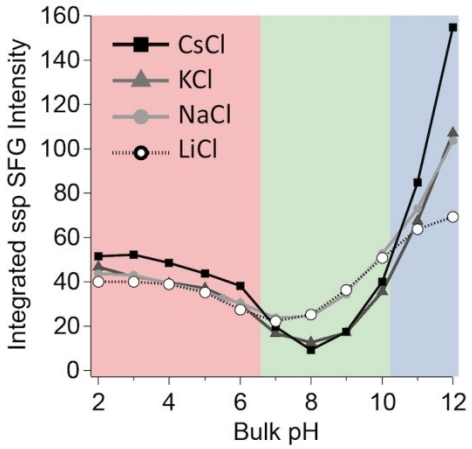

Figure 2.3. Integrated (from 2950 to 3450 cm^{-1}) ssp SFG intensities are shown for 0.5 M CsCl, KCl, NaCl and LiCl from pH 2-12 (the mean of three replicate data sets). Low, neutral and high pH regions are shaded in pink, green and blue respectively.

As observed in Figures 2.2 and 2.3, the general pH-dependent shape was the same for all four salts, with a minimum in SFG intensity (SFG_{min}) observed at pH 7-8. However, the SIE trend in I_{SFG} observed at high pH (blue region in Figure 2.3) is inverted at near-neutral pH (green region) and again at low pH (red region). Another interesting phenomenon was observed in the low pH regime below pH_{Imin}, where the SFG signal intensity increased for all four ions. For silica in pure water, as the pH is decreased, less silanol sites are deprotonated and the overall surface charge becomes less negative until the PZC is reached at pH 2-3. Due to this decreasing surface charge and early pH-dependent SHG studies of silica/water, it was assumed that the surface potential will decrease accordingly.[46] However, recent work by Darlington et al showed that SFG signal increased as the pH is lowered from a neutral to acidic pH in the presence of 0.1 M NaCl.[47] The observation of increasing signal as pH decreases from pH 8 to 2 could suggest overcharging of the surface, where the cations remain adsorbed to the silica as the pH is lower and surface charge of the silica decreases. This scenario could result in charge reversal at the silica/water interface, which is consistent with AFM results by Morag et al that suggested charge reversal of the silica surface is possible at concentrations > 0.1 M.[19] These results are also supported by Franks' 2002 study, which reported positive zeta potentials for Li^+, Na^+, K^+ and Cs^+ at 0.4 M and a study by Kosmulski which reported positive zeta potentials for 0.1 M LiCl and CsCl.[102, 109] In the results shown here, larger SFG signal intensity is observed for CsCl at low pH compared to KCl, NaCl and LiCl. These results suggest a preference for Cs^+ adsorption at low pH compared to the other cations, which is in good agreement with the findings from Morag et al.[19] Although the integrated results in Figure 2.3 provide an overview of trends in I_{SFG} for the different monovalent cations, distinguishing differences between the 3200 cm^{-1} and 3400 cm^{-1} peaks could offer further insight into structural changes arising within the EDL.

2.3.2. SFG Peak Fitting Results of Li^+ and Cs^+

It was suggested in previous studies that the two peaks arise from two different water populations, one from waters aligned near the surface within the Stern layer (3400 cm^{-1}) and the other from waters in the diffuse layer (3200 cm^{-1}).[9, 110] In our group's recent work, it was proposed that these different water populations may be experiencing different orienting forces from different surface potentials, with the 3400 cm^{-1} peak arising from waters oriented by the 0-plane potential (Φ_0) and the 3200 cm^{-1} peak arising from waters oriented by the outer Helmholtz potential, Φ_{OH}.[47] If this assumption were correct, than it would be expected that these two peaks should have different trends as a function pH, with the water molecules closest to the surface experiencing the electric field as a result of the inner Helmholtz potential and water molecules further away in the diffuse layer experiencing effects from the outer Helmholtz potential. Although integration of the water spectrum (Figure 2.3) offers insight on net water order, peak fitting must be performed in order to disentangle the behavior of the two peaks (~3200 cm^{-1} and ~3400 cm^{-1}). For simplicity, the results of LiCl and CsCl will be compared and contrasted in the following discussion. Representative peak fits of the 3200 cm^{-1} and 3400 cm^{-1} peaks are shown in Figure 2.4 for LiCl and CsCl. Peak fitting of ssp SFG spectra for LiCl and CsCl revealed that the 3200 cm^{-1} and 3400 cm^{-1} peaks exhibited different ion-specific trends (Figure 2.4). Minima in peak amplitude for the 3200 cm^{-1} peak are observed for both CsCl and LiCl, similar to the minima observed in the integrated SFG intensity plots (Figure 2.3). However, the behavior of the 3400 cm^{-1} peak is markedly different from the 3200 cm^{-1} peak, with peak amplitude remaining roughly constant for both LiCl and CsCl until pH~ 8 where CsCl increases significantly until pH~ 12 and LiCl increases slightly before decreasing again at pH >10.

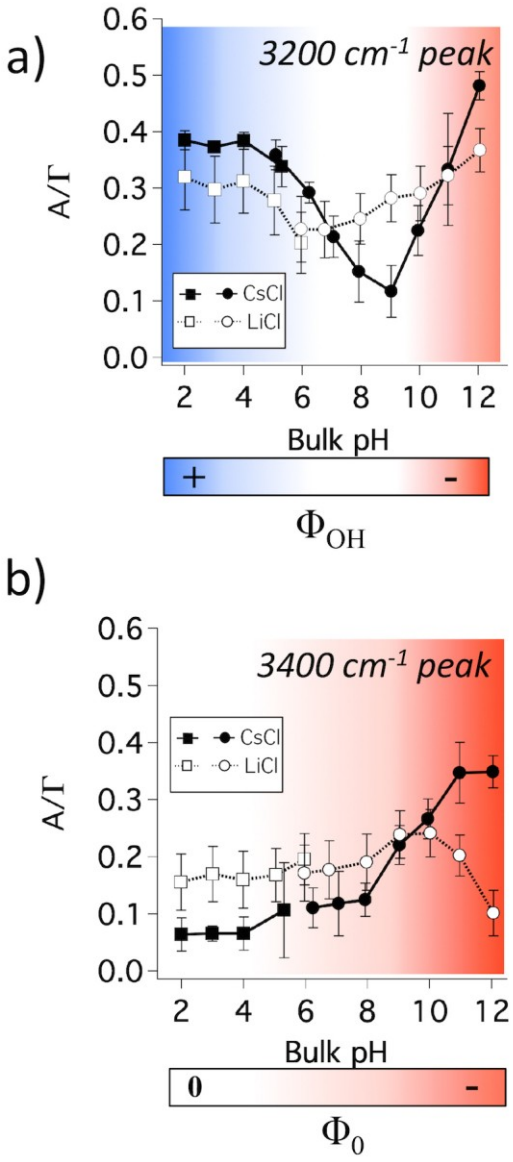

Figure 2.4. Representative peak fitting results for ssp SFG water spectra for 0.5 M CsCl and 0.5 M LiCl as a function of pH. A/Γ (proportional to the amount of ordered water) for a) the 3200 cm^{-1} peak and b) the ~3400 cm^{-1} peak are shown, where A is the peak amplitude and Γ is the homogenous line width obtained from fitting the spectra to the absolute square of summed Lorentzian functions.[1] The error bars represent one standard deviation obtained from the fits. The color scale indicates the predicted corresponding positive (blue) and negative (red) surface potentials for the OHP (a) and 0-plane (b).

In previous work, the overall trends in the 3200 cm^{-1} peak were largely attributed to changes in the Φ_{OH}, with the minimum at neutral pH corresponding to an Φ_{OH} of 0 V. Moreover, the increase in SFG intensity at lower pH was attributed to an increasingly positive Φ_{OH} (where there are more cations adsorbed at the surface than there are negative charges on the silica) and the increasing SFG intensity at high pH attributed to a more and more negative Φ_{OH} (Figure 2.4a).[47] However, the SFG results presented here indicate contributions from forces in addition to $\Phi_{OH,}$ which will be discussed.

Firstly, SIEs in the neutral region will be considered. From Figure 2.4a, it is observed that the 3200 cm^{-1} peak never reaches zero amplitude at SFG_{min}, which would be expected if Φ_{OH} was the only factor involved, indicating an additional source of water-order. Moreover, at SFG_{min}, the 3200 cm^{-1} peak for LiCl had a larger amplitude compared to CsCl, suggesting more less adsorption of Li^+ and therefore less charge screening and more alignment of water. This trend follows the predicted direct Hofmeister series of adsorption and with previous studies that have reported at pH < 7, Cs^+ adsorption is more favored than Li^+.[19, 100, 102] Furthermore, Brown and co-workers show that at pH 10 and 0.05 M salt, the position of the OHP was further away for Li^+ than Cs^+, resulting in a lower capacitance for the Stern layer that contained Li^+, which yielded a greater $|\Phi_{OH}|$ for a given charge on silica.[34] Despite the lower salt concentrations used in their experiments, the trend in A/Γ at the 3200 cm^{-1} peak observed here at pH 10 with 0.5 M salt is consistent with their findings ($Li^+ > Cs^+$). In addition, a larger 3400 cm^{-1} peak was observed for Li^+ at neutral and low pH, indicating more ordered water within the Stern layer than for Cs^+ as a result of less Li^+ adsorption (Figure 2.4b). Due to its kosmotropic properties, Li^+ is expected to reinforce the hydrogen bonding network of water molecules near it,[111] thereby inducing water order near Li^+ unrelated to Φ_{OH}. Yet, as Li^+ adsorbs on the surface, its ability to order

surrounding water may be inherently limited by the presence of the solid silica surface, resulting in more order in the water molecules on the outside of the ion facing the bulk. This asymmetry could be sufficient enough to generate non-zero SFG signals. These hydration waters of the cation would be aligned as a result of its positive charge, as opposed to water molecules in the diffuse layer that have their water dipoles aligned by negative Φ_{OH}. This would manifest in deconstructive interference of two oppositely signed peaks of different frequency (the diffuse layer waters at ~3200 cm^{-1} and the hydration waters at ~3150 cm^{-1})[112] in the SFG spectrum. Moreover, a non-zero minimum in the 3200 cm^{-1} peak would not arise at the true IEP (i.e. when $\Phi_{OH} = 0$), but when the two oppositely signed peaks are equal in amplitude. In line with this interpretation, we found that SFG_{min} was approximately 2 log units greater than the measured IEP of silica colloids in the presence of LiCl and CsCl.[102, 113] As such, due to its weak hydration and chaotropic nature, Cs^+ was expected to disrupt the H-bonding structure of water near it and therefore have a smaller contribution from asymmetric hydration than Li^+. Accordingly, Li^+ was found to have a larger contribution to the 3200 cm^{-1} Cs^+ at neutral pH (Figure 2.4a).

Next, SIEs at low pH are considered. At low pH, the 3200 cm^{-1} peak increased more for CsCl than for LiCl (Figure 2.4a), likely due to preferential adsorption of Cs^+, such that overcharging in the EDL occurred, yielding a positive Φ_{OH}, which was the dominant force for aligning water. The change in Φ_{OH} from negative to positive upon decreasing the pH from 9 to 3 has been observed previously for Cs^+.[102, 113] Owing to interactions with the surface potential and the water dipole moment, this change in sign in Φ_{OH} would cause a net flip in water orientation in the diffuse layer, possibly accounting for the red shift in the 3200 cm^{-1} peak at low pH (Figure 2.2) as previous studies on CaF_2 observed a red shift as the surface changed from negative to positive.[114] For LiCl, there is also evidence to indicate small positive Φ_{OH} at low pH.[102] However,

the presence of asymmetric cation hydration could also lead to the presence of an oppositely-signed and red-shifted peak[115] that begins to dominate the low wavenumber region as Φ_{OH} decreases in magnitude (discussed in detail in Section 2.3.4). Finally, for both LiCl and CsCl, the 3400 cm^{-1} peak decreased slightly as the pH was lowered, corresponding to a decreasing surface charge on silica and decreasing magnitude of Φ_0 as the point of zero charge was approached (Figure 2.4b).

Lastly, SIEs at high pH are examined. A clear inversion of the direct Hofmeister series was revealed at high pH, where the reverse Hofmeister series was observed ($Cs^+ < K^+ < Na^+ < Li^+$) (Figure 2.3). Moreover, the 3200 cm^{-1} peak amplitude increased dramatically with increasing pH for CsCl but began to plateau for LiCl at high pH (Figure 2.4a), indicating a large increase in $|\Phi_{OH}|$ for Cs^+ and only a moderate increase for Li^+. This suggests a change in adsorption at pH <10 where Cs^+ adsorbed more than Li^+, but at pH >10, Cs^+ was driven away from the surface and Li^+ adsorption was favored. This expulsion of Cs^+ would lead to a lower capacitance for Cs^+ than Li^+ at pH >10 as the distance of the OHP from the silica surface increased. As the capacitance is inversely related to $|\Phi_{OH}|$ for a given charge on silica, this inversion of the capacitance results in an inversion of Φ_{OH}, where $|\Phi_{OH,Li+}| < |\Phi_{OH,Cs+}|$. These results agree with previous studies that inferred Cs^+ is repelled from the charged surface at high pH while the adsorption of smaller ions (Na^+ and Li^+) is favored, [19, 98, 116] which was attributed to displacement of Cs^+ at the OHP by water molecules that more strongly hydrogen bond to the increasingly deprotonated silica.[19] The observed changes in the A/Γ of the 3400 cm^{-1} peak were consistent with expulsion of Cs^+ from the Stern layer. For CsCl, the 3400 cm^{-1} peak increased from pH 2-11, which was expected as the surface, and with it Φ_0, became more negative, leading to more water alignment within the Stern layer. However, the significant increase from pH 8 to

11 could also suggest an increase in the amount of water near the surface, consistent with repulsion of Cs^+. Yet in the case of LiCl, the 3400 cm^{-1} peak increased only slightly, and then began to decrease at pH > 10 (Figure 2.4b), suggesting that LiCl was specifically adsorbed at high pH, displacing water near the surface (also resulting in a greater capacitance and smaller 3200 cm^{-1} mode). Specific adsorption of Li^+ is supported by molecular dynamics simulations that have predicted that the small kosmotropic ion, Na^+, may lose its hydration shell and preferentially adsorb to the silica surface at high pH, whereas Cs^+ likely retains its hydration shell and resides further away from the surface at high surface charge densities.[98] A schematic of the combination of these factors thought to account for the observed pH-dependent trends for both the 3200 cm^{-1} and 3400 cm^{-1} peaks are shown in Figure 2.5 as well as an expanded equation that describes the source of SFG intensity. It should be noted that for many of the previous studies cited, with the exception of the AFM experiments by Morag, SIEs were only considered for a single pH. The results presented here demonstrate that SIEs for silica are highly pH dependent and indicate that capacitance values used in EDL models are only appropriate for a narrow pH range.

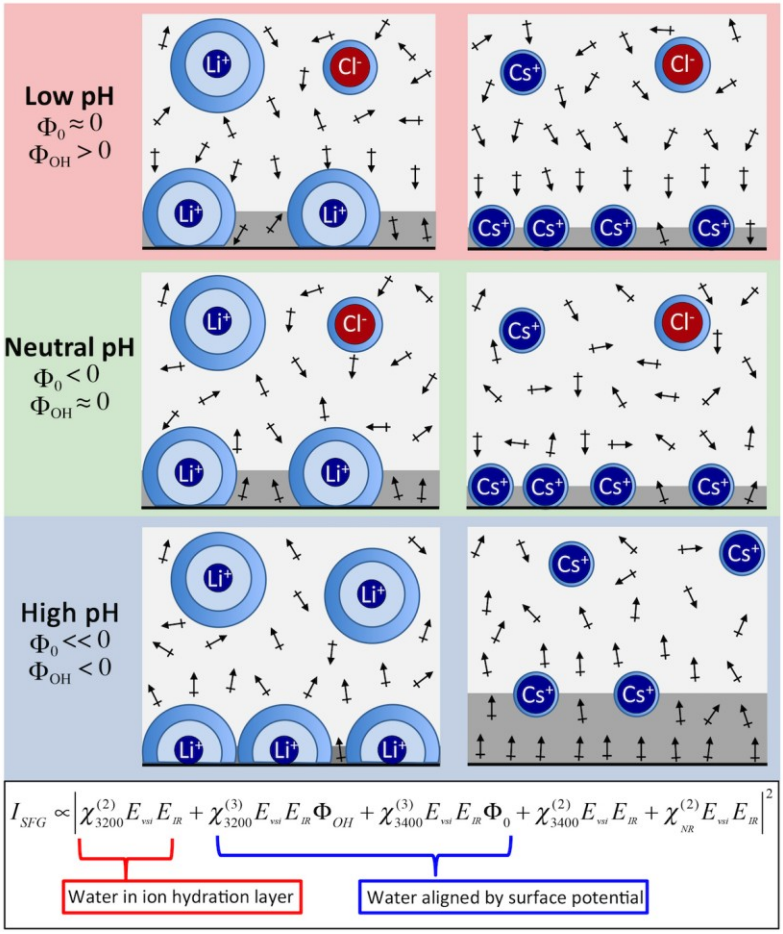

Figure 2.5. Schematic of Li^+ (left) and Cs^+ ions (right) in the EDL at the silica/water interface and corresponding alignment of water dipoles (arrows, not to scale). The silica surface is shown as a black line, the Stern layer is shown in grey, cation hydration layers in light blue and Cl^- counter ions in red. The expression describing SFG intensity is expanded to include contributions from surface potentials and cation hydration. $\chi^{(2)}_{3400}$ will also change as the number of water molecules within the Stern layer changes.

From the equation 1.11 from Chapter 1, the intensity of the SFG is expressed as: $I_{SFG} \propto \left|\chi^{(2)} E_{VIS} E_{IR} + \chi^{(3)} E_{VIS} E_{IR} \Phi_0\right|^2$, where the first term, $\chi^{(2)} E_{VIS} E_{IR}$, denotes the interfacial water molecules that are present at the silica/aqueous interface that are are not aligned by the surface potential, and the second term, $\chi^{(3)} E_{VIS} E_{IR} \Phi_0$, denotes the interfacial water molecules that are aligned by the surface potential. From the SFG results obtained in this Chapter 2, the equation can be further expanded such that:

$$I_{SFG} \propto \left|\chi^{(2)}_{3200} E_{VIS} E_{IR} + \chi^{(3)}_{3200} E_{VIS} E_{IR} \Phi_{OH} + \chi^{(3)}_{3400} E_{VIS} E_{IR} \Phi_0 + \chi^{(2)}_{3400} E_{VIS} E_{IR}\right|^2 \qquad \text{(Equation 2.1)}$$

$\chi^{(3)}_{3200} E_{VIS} E_{IR} \Phi_{OH}$ comes from the interfacial water molecules aligned by the outer Helmholtz potential in the diffuse layer, $\chi^{(3)}_{3400} E_{VIS} E_{IR} \Phi_0$ comes from the interfacial water molecules aligned by the surface potential within the Stern layer, and $\chi^{(2)}_{3200} E_{VIS} E_{IR} + \chi^{(2)}_{3400} E_{VIS} E_{IR}$ comes from the interfacial water molecules within the hydration layer of the cation and/or interfacial water molecules that are not affected by the surface potential and are likely hydrogen bonded to the silica surface.

To relate these two different populations to changes in the EDL, the spectral intensity (I_{SFG}) were fit to the sum of two Lorentzians as shown in the following equation:

$$I_{SFG} = \left| \frac{A_{3200\,peak}}{\omega_{IR} - \omega_{3200\,peak} + i\Gamma} + \frac{A_{3400\,peak}}{\omega_{IR} - \omega_{3400\,peak} + i\Gamma} + NR \right|^2 \qquad \text{(Equation 2.2)}$$

where, A is the peak amplitude, ω_{IR} is the frequency of the incident IR light, ω is the peak frequency, Γ is the linewidth, and NR is the non-resonant term.

Putting equation 2.1 and equation 2.2 together, we have:

$$\left|\chi^{(2)}_{3200}E_{VIS}E_{IR} + \chi^{(3)}_{3200}E_{VIS}E_{IR}\Phi_{OH} + \chi^{(3)}_{3400}E_{VIS}E_{IR}\Phi_0 + \chi^{(2)}_{3400}E_{VIS}E_{IR}\right|^2$$
$$\propto \left[\frac{A_{3200\,peak}}{\omega_{IR} - \omega_{3200\,peak} + i\Gamma} + \frac{A_{3400\,peak}}{\omega_{IR} - \omega_{3400\,peak} + i\Gamma}\right]^2 \qquad \text{(Equation 2.3)}$$

With $E_{VIS}E_{IR}$ being constant, $A_{3200peak}$ is proportional to $\chi^{(2)}_{3200} + \chi^{(3)}_{3200}\Phi_{OH}$ and gives information about interfacial water molecules within the diffuse layer, and $A_{3400peak}$ is proportional to $\chi^{(3)}_{3400}\Phi_0 + \chi^{(2)}_{3400}$ and gives information about interfacial water molecules within the Stern layer. As will be discussed in Section 2.3.4., the amplitude can be further related to the number of aligned water molecules through $\chi^{(2)}$ and $\chi^{(3)}$.

2.3.3. SFG Data with the pss Polarization Combination at High pH

It has been shown that the pss polarization combination is most sensitive to the 3400 cm^{-1} peak in the water spectrum, with little contribution from the 3200 cm^{-1} peak.[47] Therefore we performed pss SFG experiments for 0.5 M CsCl and LiCl from pH 6-12 to observe whether the trends observed at high pH for the 3400 cm^{-1} peak in the ssp SFG spectrum were also consistent with those observed in the pss spectrum, the results of which are shown in Figure 2.6. In the reported ssp peak fitting results (Figure 2.4), distinct specific ion trends were observed in the 3400 cm^{-1} peak between LiCl and CsCl at high pH, where from pH 8, the peak amplitude for CsCl increased with increasing pH, but for Li the peak amplitude increased slightly from pH 8 to pH 10, but began to decrease again from pH 10 -12. This same trend was observed in the pss results shown in Figure 2.6, where the 3400 cm^{-1} peak increased for from pH 7-12 for CsCl and increased from pH 6-10 and then decreased from pH 10 -12 for LiCl. The similarities in the 3400 cm^{-1} peak behavior as a function of pH for the two different polarization combinations indicate

that the source of 3400 cm^{-1} peak in the ssp spectrum also contributes to the source of the 3400 cm^{-1} peak in the pss spectrum.

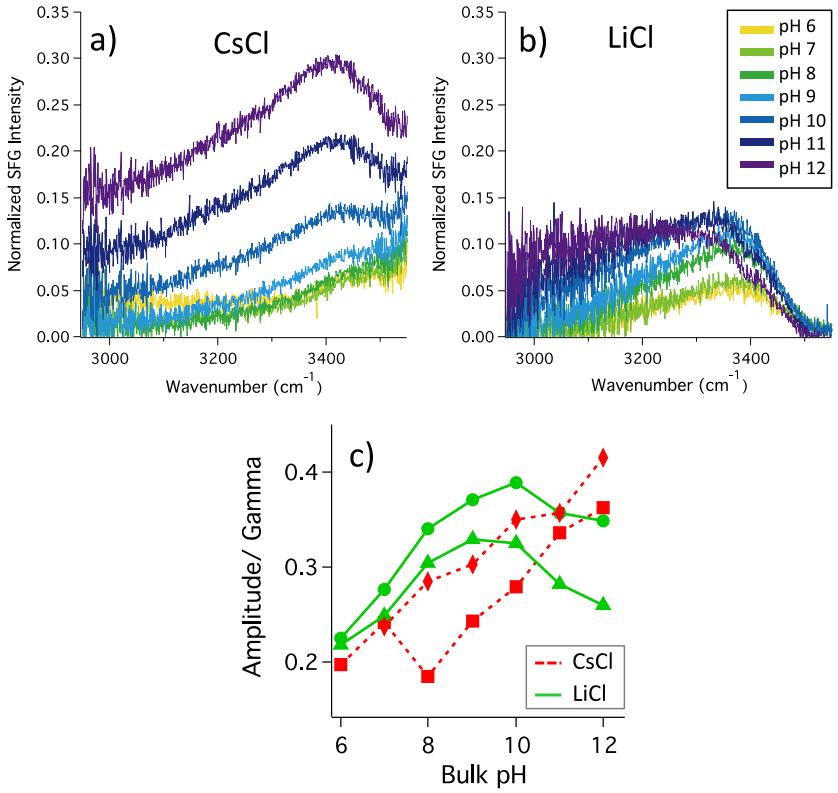

Figure 2.6. Unsmoothed, gold normalized pss SFG spectra are shown for a) 0.5 M LiCl and b) 0.5 M CsCl from pH 6 – 12. Peak fitting results of two replicate pss SFG data sets are also shown in for the 3400 cm^{-1} peak c).

2.3.4. Predictions of the Effect of Ion Hydration and Charge Reversal on SFG Intensity

From the peak fitting results shown in Figure 2.4, we observe that SFG_{min} is nonzero suggesting additional contribution from interfacial water molecules other than the interfacial water molecules aligned due to surface potential. We also observe that SFG_{min} for Cs^+ is much smaller than Li^+ and the peak at ~3200 cm^{-1} starts to red-shift to ~3150 cm^{-1} at low pH. We

attributed the nonzero SFG_{min} to the interfacial water molecules within the asymmetric hydration layer of the cation. To verify that hydration layer could account for the red-shift and the sources of these nonzero SFG_{min}, we use the sum of three Lorentzians shown in equation 2.4 to simulate the peak occurring at ~3200 cm^{-1} ($A_{3200peak}$).

$$I_{SFG} = \left| \frac{A_{peak1}}{\omega - \omega_{peak1} + i\Gamma_{peak1}} + \frac{A_{peak2}}{\omega - \omega_{peak2} + i\Gamma_{peak2}} + \frac{A_{peak3}}{\omega - \omega_{peak3} + i\Gamma_{peak3}} + NR \right|^2 \qquad \text{(Equation 2.4)}$$

First, we will relate I_{SFG} to the amplitude of each of the three peaks and also relate it to the number of aligned water molecules at the silica/aqueous interface. From equation 2.3, we have shown that $A_{3200peak}$ is proportional to $\chi^{(2)}_{3200} + \chi^{(3)}_{3200}\Phi_{OH}$ where 3200 cm^{-1} is the OH stretching wavenumber coming predominantly from the interfacial water molecules within the diffuse layer at the silica/aqueous interface. To relate the above equation to the number of interfacial water molecules, we first consider equation 1.2 from Chapter 1, $\chi^{(3)}\Phi = N_{H_2O}\left(\frac{\mu_{H_2O}\Phi}{bkT}\right)\beta_{H_2O} + N_{H_2O}\gamma_{H_2O}\Phi$, where the $N_{H_2O}\gamma_{H_2O}\Phi$ term was assumed to be small and negligible owing to the small value of γ_{H_2O}. Additionally, $\chi^{(2)}$ can be related to the number of aligned interfacial water molecules according to $\chi^{(2)}_R = N_{H_2O} < \beta_{H_2O} >$ as shown in equation 1.13 from Chapter 1. Thus, $\chi^{(2)}_{3200} + \chi^{(3)}_{3200}\Phi_{OH}$ can be further expanded such that:

$$A_{3200\,peak} \propto \chi^{(2)}_{3200} + \chi^{(3)}_{3200}\Phi_{OH} \propto N_{3200} < \beta_{3200} > + N_{3200}\left(\frac{\mu_{H_2O}\Phi}{bkT}\right)\beta_{3200} \qquad \text{(Equation 2.5)}$$

where β_{3200} is the molecular hyperpolarizability of the 3200 cm^{-1} mode. In this simulation, peak 1 corresponds to water in the diffuse layer aligned by a negative outer Helmholtz potential (oxygen pointed towards the bulk). Peak 2 corresponds to water in the diffuse layer aligned by a

positive outer Helmholtz potential (hydrogens pointed towards the bulk). Peak 3 corresponds to water in the cation hydration layer (leading to hydrogens pointed towards the bulk). Therefore, from equation 2.4 and equation 2.5, we can further expand each of the three peaks that are contributing to the peak at ~3200 cm^{-1} as:

$$A_{peak1} \propto N_{3200}\left(\frac{\mu_{H_2O}\Phi}{bkT}\right)\beta_{3200} \quad \text{(Equation 2.6)}$$

$$A_{peak2} \propto N_{3150}\left(\frac{\mu_{H_2O}\Phi}{bkT}\right)\beta_{3150} \quad \text{(Equation 2.7)}$$

$$A_{peak3} \propto N_{3150} < \beta_{3150} > \quad \text{(Equation 2.8)}$$

To account for the red-shift, we assumed that water aligned by a positive potential has a slightly different wavenumber (~3150 cm^{-1}). Similarly, previous SFG studies have suggested hydrated cations have a resonance closer to ~3150 cm^{-1}.[112]

In our simulation, the sign of A_{peak1} is arbitrarily set to be positive with β_{3200} being positive and μ_{H_2O} negative when water molecules are oriented with their oxygen pointing towards the bulk solution as a result of the negative Φ. By definition, β is nonzero when there is a break in inversion symmetry. As such, when water molecules in the diffuse layer flip by 180º due to a change in the sign of outer Helmholtz potential, both β and μ_{H_2O} change sign. The sign of A_{peak2} is therefore negative because β_{3150} is now negative, μ_{H_2O} is positive, when water is oriented with hydrogens pointing towards the bulk solution as a result of a positive Φ. The sign of A_{peak3} is also negative because β_{3150} is negative, when water in the asymmetric cation

hydration layer is oriented towards a cation with its hydrogens pointing towards the bulk solution. Since A_{peak1} has an opposite sign from A_{peak2} and A_{peak3}, these peaks interfere destructively.

To summarize, we propose that three peaks could be contributing to the broad peak observed at ~3200 cm^{-1} 1) a positive peak at 3200 cm^{-1} that corresponds to waters in the diffuse layer aligned with their hydrogen atoms pointing towards the surface by the negative Φ_{OH} 2) A negative red shifted peak at ~3150 cm^{-1} from waters in the diffuse layer with their hydrogens pointed away from the surface aligned by a positive Φ_{OH} and 3) A negative red shifted peak at ~3150 cm^{-1} corresponding to waters within the hydration layer of the cation ordered by kosmotropic nature of the ion. As the pH decreases, the surface charge and $|\Phi_{OH}|$ decreases. As such, it is expected that the peak amplitude of peak 1 (A_{peak1} at 3200 cm^{-1}) will decrease. When Φ_{OH} is negative, it is expected that peak 2 (A_{peak2} at 3150 cm^{-1}) is zero. However, if Φ_{OH} becomes positive from overcharging, the magnitude of peak 2 should increase and be opposite in sign to peak 1, which is now zero. If peak 3 represents the hydration of the cation, it is expected to remain constant for as long as the ion is present at the surface and be opposite in sign to peak 1 as the waters will be oriented with their hydrogens pointing towards the cation. This peak is also expected to be red-shifted from waters in the diffuse layer, with a frequency ~ 3150 cm^{-1}.[112] Figure 2.7 shows the predicted shape and intensity trend for these three predicted interfering Lorentzian peaks. Similar to the experimental SFG spectra as a function of pH, as the intensity of A_{peak1}, peak occurring at ~3200 cm^{-1}, decrease, the predicted SFG intensity decreases. However, a minimum in predicted intensity is observed when A_{peak1} equals A_{peak3}, the amplitude of the constant hydration peak at 3150 cm^{-1} (shown in red). In addition, the intensity of the signal at the minimum is greater when the A_{peak3} is greater than A_{peak1}. As the amplitude of the hydration peak (A_{peak3}) becomes larger in amplitude than the amplitude of the 3200 peak, A_{peak1}, the predicted

signal begins to increase again, but red shifted. The appearance of peak 2, the red-shifted negative peak as a result of positive Φ_{OH} at low pH, also contributes to the increase in the amplitude of the red shifted peak. Simulations of these interfering modes revealed that the larger signal at SFG_{min} for Li^+ could be described by a larger contribution from water within the cation hydration layer and also the increase in SFG signal and red shift in the 3200 cm^{-1} peak at low pH was attributed to contributions from asymmetric cation hydration effects and overcharging of the EDL.

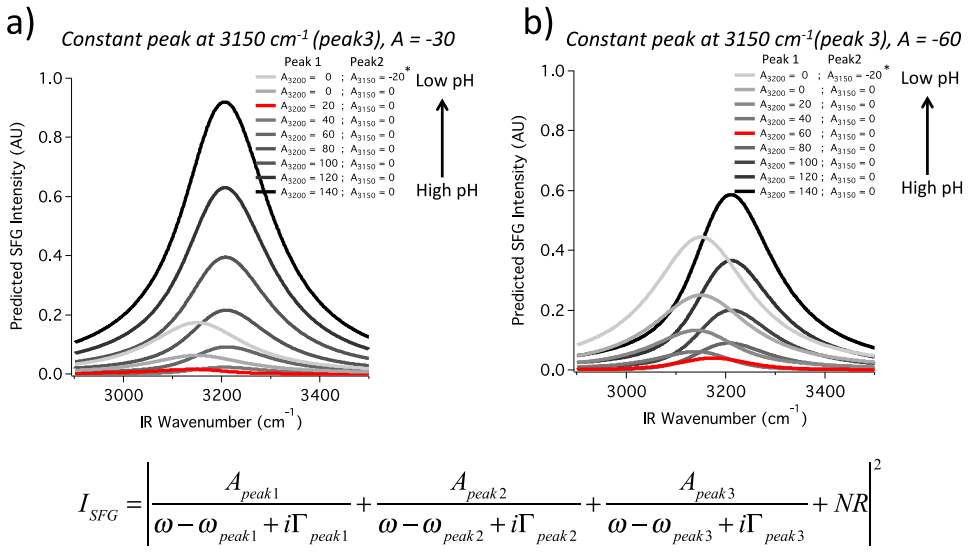

$$I_{SFG} = \left| \frac{A_{peak1}}{\omega - \omega_{peak1} + i\Gamma_{peak1}} + \frac{A_{peak2}}{\omega - \omega_{peak2} + i\Gamma_{peak2}} + \frac{A_{peak3}}{\omega - \omega_{peak3} + i\Gamma_{peak3}} + NR \right|^2$$

Figure 2.7. Predicted SFG intensity for 3 interfering peaks with different amplitudes (Γ = 120 cm^{-1} for all peaks). The peak amplitude of the constant peak at 3150 cm^{-1} is a) -30 and b) -60. The spectrum where the minimum in predicted SFG intensity occurs is shown in red. * indicates where overcharging of the EDL occurs. The equation used to simulate the interfering peaks is also shown.

2.4. Conclusion

Vibrational SFG spectroscopy revealed pH-dependent SIEs for CsCl, KCl, NaCl and LiCl at 0.5 M concentrations. The observed SIEs indicate that cation adsorption at the silica/water interface is highly dependent on the cation type as well as pH. Clear differences in pH-dependent trends in the two peaks in SFG water spectra were observed for LiCl and CsCl, which were attributed to different aligning forces acting on two unique water populations: Φ_{OH} for the diffuse layer water molecules (3200 cm^{-1}) and Φ_0 for water close to the silica surface in the Stern layer (3400 cm^{-1}). Trends in the SFG spectra indicate strong adsorption of Cs^+ and weaker adsorption of Li^+ occurs at pH <10. A reversal of these trends was observed at pH >10, which was attributed to expulsion of Cs^+ from the silica surface and strong adsorption of Li^+. In addition, nonmonotonic behavior was observed in integrated SFG spectra and 3200 cm^{-1} peak intensity. The increase in SFG signal and red shift in the 3200 cm^{-1} peak at low pH was attributed to contributions from asymmetric cation hydration effects and overcharging of the EDL. The results shown here provide insight into inconsistencies among previous SFG experiments that examined single pH points and provide further evidence that pH-dependent trends in SFG spectral shapes and in particular the intensities are likely due to a combination of Φ_0, Φ_{OH}, interfacial cation hydration and pH-dependent changes in cation affinities for silica.

Chapter 3

Specific anion effects at the silica/aqueous interface:

A comparison of bicarbonate and chloride

3.1. Introduction

Silica is one of the most abundant materials on earth, and, as such, understanding the properties of the silica/water interface is critical in understanding many environmental and geochemical processes, such as pollutant transport and weathering, mineral precipitation, and ocean acidification.[117-119] The adsorption of different ions on silica sands were shown to vary under different environment conditions such as pH, and the type of ions present.[33, 51, 120] In the previous chapter, we studied the effect of various monovalent cations on the structure of interfacial water molecules at the silica interface, and our results showed that the hydration shell and size of the ion played an important role in how well it interacted with the silica surface and influenced the water structuring at the surface. In this chapter, the effect of sodium bicarbonate at the silica/aqueous interface was studied with a focus on how the bicarbonate anion specifically influences the structure of water at the interface in comparison to the chloride anion.

Sodium (Na^+) and bicarbonate (HCO_3^-) are two of the most commonly found ions in natural water.[119, 121-122] Moreover, weathering of silicate minerals has also shown to cause higher concentration of bicarbonate in ground water.[119] The bicarbonate ion, HCO_3^-, is also one of the most commonly found ions in industrial water recycling processes, including oil sands tailings ponds.[4-5, 123-126] $NaHCO_3$ is known to promote dispersion in clays and also improve bitumen recovery in the oil sands.[5, 123] Thus, it is of great interest to study the properties of bicarbonate and its interactions with water and silica.

Past studies have shown that HCO_3^- stabilizes sand/clay dispersions in silica oil sands due to its tendency to adsorb to silica/aqueous interface.[5, 123-129] For example, Koltyar et al. showed

that HCO_3^- has a tendency to adsorb to silica surface and hinder the tailings pond reclamation processes.[123] In this study, it was found that in the presence of 20 mM NaCl solution, clays aggregated over time whereas under the presence of 20 mM $NaHCO_3$, the clay remained in suspensions as a result of HCO_3^- adsorption.[123] Although the interaction of HCO_3^- and silica can hinder clay and silica settling, Zhao et al. has also shown that the presence of HCO_3^- improved bitumen extraction by making both the surface of oil sand grains and the bitumen more negatively charged.[5] They measured the zeta potential of poor processing oil sands ores and showed that the presence of HCO_3^- led to more negative zeta potential.[5] They also did AFM measurements and showed that the adhesion forces between bitumen and the sand grains decreased with the presence of HCO_3^-, which further supports that HCO_3^- can act as a dispersant and promote the separation of bitumen from oil sands by adsorbing to both silica and bitumen surface.[5] It is interesting to note that HCO_3^- is attracted towards negatively charged surface such as silica despite being an anion. This tendency of HCO_3^- to stay close to the negatively charged silica surface can possibly be linked to its weak water structure making properties.

Ozdemir et al measured the viscosity and FTIR transmission of various carbonate and bicarbonate salts (Na_2CO_3, K_2CO_3, $NaHCO_3$ and NH_4HCO_3) in 4 wt% D_2O in H_2O mixtures.[125] By adding a small amount of D_2O, they ensured that a rapid exchange has occurred between H and D atoms to form HOD molecules such that they do not observe any intramolecular interactions between OH or OD stretches within a water molecule. Salts which increase the viscosity of aqueous solutions are considered structure makers and those which decrease the viscosity are considered structure breakers.[125, 130] OD stretching frequencies of water molecules give information about intermolecular vibrational motions and the interaction between the ions in solution and water molecules such that an increase in hydrogen bonding strength causes the OD

stretching frequencies to shift to lower wavenumbers.[125, 130] Their viscosity results show that Na_2CO_3 increased the viscosity of salt solution and has very strong water structure making effects while $NaHCO_3$ did not significantly change viscosity.[125] Their FTIR results also showed that CO_3^{2-} increased the width of OD bands of the solution with its peak shifting to lower wavenumbers whereas no significant change was observed for HCO_3^- which suggests that CO_3^{2-} has great water structure making properties whereas HCO_3^- has weak water structure making properties. These results seem to suggest that HCO_3^- has propensity to interact with hydrophobic surfaces due to its weak water structure making properties. In other words, the tendency of HCO_3^- to promote weakly structured hydrogen bonding of water molecules may cause it to interact more strongly with the hydrophobic surface than the bulk water. In fact, Du et al performed molecular simulations of sodium bicarbonate and carbonate ions at the air/aqueous interface and found that sodium and bicarbonate ions remained closer to this hydrophobic interface whereas carbonate ions were typically further away from the interface.[131] In the case of silica/water surface, HCO_3^- will likely have stronger interaction with the hydroxylated part of amorphous fused silica surface, which exhibits hydrophobic character.[80]

Nonlinear optical (NLO) methods have been used previously to study the effect of HCO_3^- on water structure. Allen and co-workers studied the orientation of water molecules at the air/aqueous interface of aqueous Na_2CO_3 and $NaHCO_3$ solutions using phase-sensitive SFG. Their results showed that HCO_3^- did not significantly perturb the interfacial water structure whereas CO_3^{2-} caused the interfacial water molecules to orient themselves such that its hydrogen atoms are pointing towards the bulk water.[129] They suggested that a weakly ordered water structure is formed at the surface of $NaHCO_3$ solution and HCO_3^- and Na^+ intercalate in the hydrogen bonding environment within the first few layers of the air/water surface whereas CO_3^{2-}

stays further away from the surface and thereby increases the interfacial thickness (i.e. the region where there is a break in inversion symmetry).[129] However, this study examined the water structure making/breaking effects of HCO_3^- at the air/aqueous interface only. The studies performed in this chapter are aimed at bridging the gap between these NLO studies at the air/aqueous interface and previous studies on HCO_3^- adsorption on silica. The investigation of the effects of HCO_3^- on the silica/ aqueous interface using SFG and SHG methods should allow an assessment of ion adsorption and corresponding effects on interfacial water structure.

Given this preliminary evidence of bicarbonate ion adsorption on silica and its weak "structure making" effects, in this chapter, we would like to further investigate bicarbonate adsorption on silica and in particular how adsorbed bicarbonate ions affects the acid/base chemistry of silica/aqueous interface. We are especially interested in determining how bicarbonate ions affect the interfacial structure of water at silica. There have not been any studies that looked at the effect of bicarbonate ion on structuring of water molecules at the silica/water interface. Therefore in this chapter, we first used SFG spectroscopy to investigate the adsorption behaviour of HCO_3^- at silica and to probe its effect on the molecular structure of interfacial water. SHG measurements were also performed as a complement to SFG to study the effect of HCO_3^- on the surface charge density of silica.

3.2. Equilibrium Reaction of Bicarbonate in Water

Carbonate equilibrium is a major buffer system that influences the pH of the water, where water is in equilibrium with carbon dioxide in the atmosphere. [118, 132-134] In lakes or oceans, most dissolved carbon dioxide reacts with water and establishes the carbonate equilibrium.[133-134] First,

CO_2 gas dissolves in water. The equilibrium constant K_{CO2} is a measure of the solubility of CO_2 gas in water (Equation 3.1).[133-134]

$$CO_{2(g)} \xleftrightarrow{K_{CO_2}} CO_{2(aq)} \ , \ K_{CO_2} = 10^{-1.5} \qquad \text{(Equation 3.1)}$$

Once carbon dioxide is dissolved in solution, it reacts with water to produce carbonic acid. (Equations 3.2-3.3).[133-134]

$$CO_{2(aq)} + H_2O \xleftrightarrow{K_{eq}} H_2CO_{3(aq)}, \ K_{H_2CO_3} = 10^{-2.8} \qquad \text{(Equation 3.2)}$$

$$K_{CO_2} K_{H_2CO_3} = \frac{[H_2CO_3]}{P_{CO_2}} \qquad \text{(Equation 3.3)}$$

Carbonic acid reacts with water and first dissociates into bicarbonate ion and releases a proton (Equation 3.4).[133-134]

$$H_2CO_{3(aq)} + H_2O \xleftrightarrow{K_{a1}} H_3O^+ + HCO_3^{-}{}_{(aq)}, \ K_{a1} = 10^{-6.4} \qquad \text{(Equation 3.4)}$$

Bicarbonate can further react with water to release another proton and generate carbonate ion (Equation 3.5).[133-134]

$$HCO_3^{-}{}_{(aq)} + H_2O \xleftrightarrow{K_{a2}} H_3O^+ + CO_3^{2-}{}_{(aq)}, \ K_{a2} = 10^{-10.3} \qquad \text{(Equation 3.5)}$$

Depending on the pH of the system, different carbonate species exist. Equation 3.4 and equation 3.5 can be used and rearranged to solve for the fraction of $[H_2CO_3]$, $[HCO_3^-]$, and $[CO_3^{2-}]$ at chemical equilibrium under a wide range pH.

$$\frac{[H_2CO_3]_{eq}}{Total} = \frac{[H^+]_{eq}^2}{[H^+]_{eq}^2 + K_{a1}[H^+]_{eq} + K_{a1}K_{a2}} \qquad \text{(Equation 3.6)}$$

$$\frac{[HCO_3^-]_{eq}}{Total} = \frac{K_{a1}[H^+]_{eq}}{[H^+]_{eq}^2 + K_{a1}[H^+]_{eq} + K_{a1}K_{a2}} \qquad \text{(Equation 3.7)}$$

$$\frac{[CO_3^{2-}]_{eq}}{Total} = \frac{K_{a1}K_{a2}}{[H^+]_{eq}^2 + K_{a1}[H^+]_{eq} + K_{a1}K_{a2}} \qquad \text{(Equation 3.8)}$$

$$Total = [H_2CO_3]_{eq} + [HCO_3^-]_{eq} + [CO_3^{2-}]_{eq} \qquad \text{(Equation 3.9)}$$

Figure 3.1 shows the mole fraction of bicarbonate present at different pH under closed system with specified total carbonate concentration.[133-134]

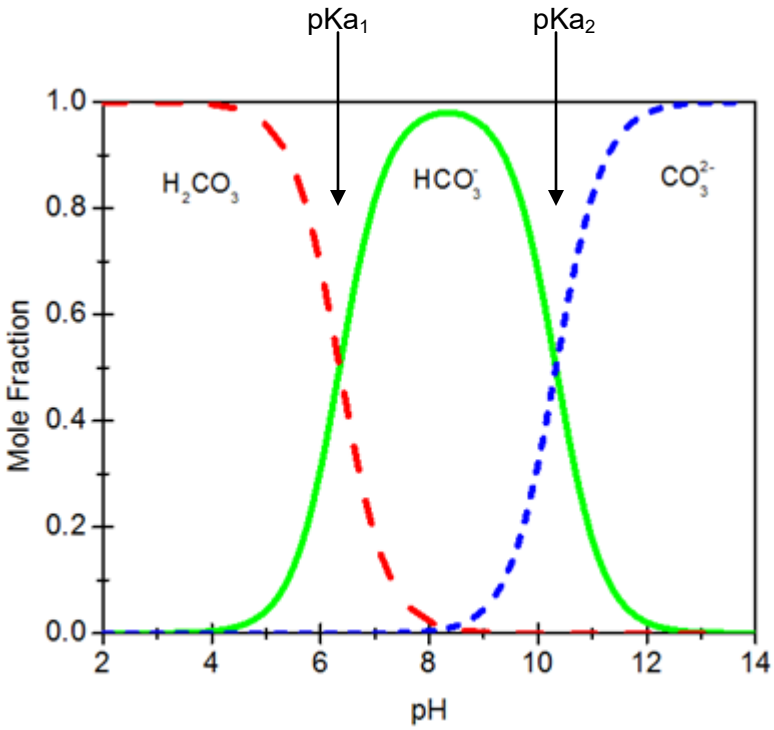

Figure 3.1. Mole fraction of bicarbonate under a wide range pH in pure water at 25ºC.[133] This graph was re-drawn based on the plot from reference 133.

H_2CO_3, HCO_3^-, CO_3^{2-}, H^+ and OH^- exist in the carbonate-water system.[118, 132-134] At pH<pK_{a1} (6.4), H_2CO_3 is dominant in solution.[133] When the pH is in between pK_{a1} (6.4) and pK_{a2} (10.3), HCO_3^- is predominant in solution.[133] At pH>pK_{a2} (10.3), CO_3^{2-} is predominant. Figure 3.1 shows that bicarbonate is most predominant at around pH 8.[133]

In this chapter, we measured the SFG of 0.1 M $NaHCO_3$ from pH 8-5 and SHG from pH 8-2 but still focused in the pH 8-5 region where HCO_3^- is predominant in the solution (Figure 3.1). The SHG and SFG of an aqueous NaCl sample under the same experimental conditions were measured and compared with the $NaHCO_3$ results to identify any specific effects that could arise due specifically to the presence of HCO_3^-. SHG and SFG techniques were used to study the HCO_3^- effects at silica/aqueous interface and confirm two properties of HCO_3^- which have been shown in previous research: adsorption of bicarbonate to the silica/aqueous interface and whether it has tendency to form weak water structure making properties.[5, 123, 125-126, 128-129]

3.3. Experimental

3.3.1. Laser System and SHG Line.

Experimental setup for the SHG laser system is shown in Figure 3.2. First, femtosecond Ti:sapphire oscillator (Spectra-Physics, Mai Tai, 80 MHz) and a Nd:YLF laser (Spectra-Physics, Empower) was used to seed and pump a regeneratively amplified laser (Spitfire Pro, Spectra Physics, 1kHz, 100 fs, 3.3 W) to generate an 800-nm beam. Then, the direct output from the Spitfire ($\lambda = 800 \pm 2$ nm) was passed through a neutral-density filter (New Focus, cat. # 5215) to be attenuated around 0.8 ± 0.1 μJ per pulse which was directed through a half-wave plate (HWP) and polarizer for s-polarization selection. The s-polarized light was then focused onto the fused silica/water interface at an angle of 62° near total internal refraction from surface normal. The reflected second harmonic light generated at the interface was then passed through a color glass filter (Thorlabs) to remove any reflected fundamental light and passed through another polarizer for p-polarization selection and was focused onto a monochromator (Optometrics Corp., Mini-

Chrom MC1-02) tuned to the second harmonic wavelength (400 nm). Selected SHG light (400nm) was then detected by a photomultiplier tube (PMT, Hamamatsu Photonics) and the amplified electric response was counted with a gated photon counter (Stanford Research Systems). Before performing each experiment, the quadratic power dependence and SHG wavelength dependence were verified to ensure that we are measuring the SHG signal. For all SHG measurements, a freshly cleaned fused silica hemisphere (Almaz optics, 1 inch diameter, IR-grade SiO_2) was placed on a custom-built Teflon cell so that the flat surface of the hemisphere was in contact with the aqueous phase. The top of the sample cell was exposed so that the salt solution could be replaced with water and the pH of the sample solution can be routinely changed and monitored from the top opening.

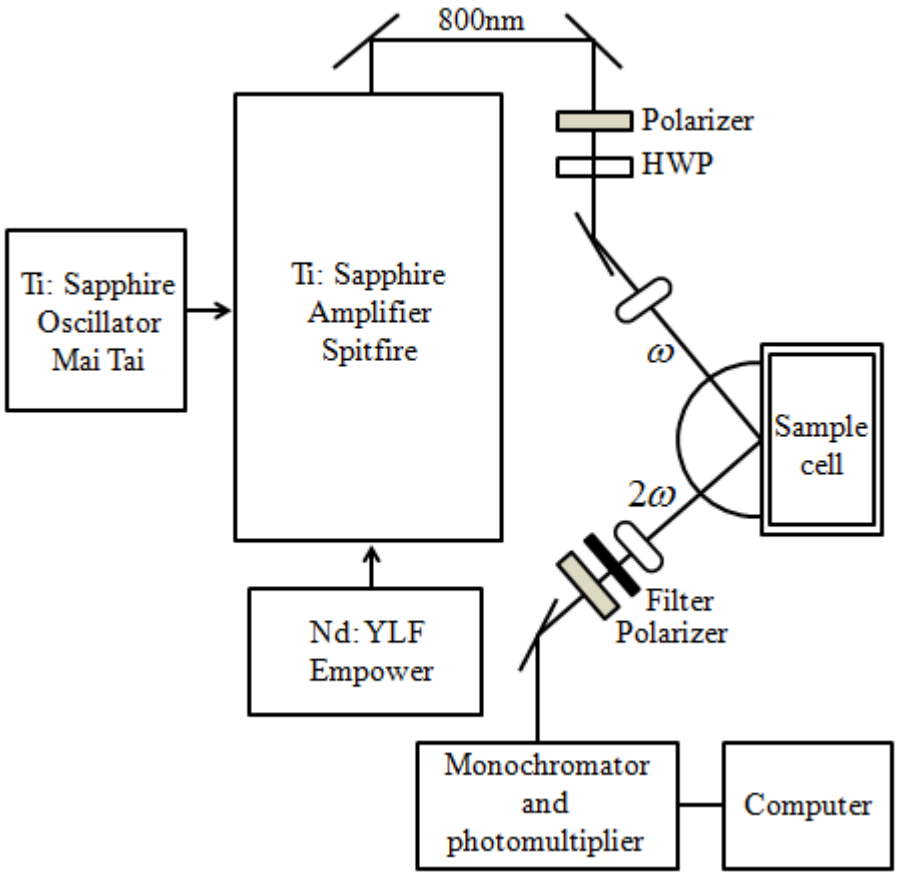

Figure 3.2. Schematic diagram of SHG laser system.

3.3.2. Laser System and SFG Line.

Experimental setup for the SFG laser system is shown in Figure 3.3. Two-thirds of the Spitfire output (800 nm, 2.2 W) was used to pump a TOPAS-C/NDFG optical parametric amplifier (Light Conversion). The resulting broadband infrared light was tuned in the range of 2750 – 3300 nm to probe the OH stretching frequency of the interfacial water molecules. The visible light from the Spitfire (100 fs, λ = 800 nm) was broadened to a picosecond pulse (FWHM ~ 10 cm^{-1}) using a Fabry-Perot etalon. The femtosecond s-polarized or p-polarized IR light (∼20−25 μJ/pulse) and the picosecond visible light (∼10 μJ/pulse) which passed through a half-wave plate (HWP) and polarizer were overlapped spatially and temporally onto the fused silica/aqueous interface at angles of 66° and 64°, respectively, from surface normal to generate the sum frequency light. The reflected SFG light was recollimated and filtered with a bandpass filter (Chroma, HQ 617/70 M) to remove any residual 800nm visible light and then passed through a polarizer to select s-polarized or p-polarized light. The filtered and polarized SFG light was then focused onto a spectrograph (Acton SP-2556 imaging spectrograph, grating: 1800 grooves/mm with 500 nm blaze wavelength), which was connected to a charge coupled device camera (Acton PIXIS 100B CCD digital camera system, 1340 × 100 pixels, 20 μm × 20 μm pixel size, Princeton Instruments).

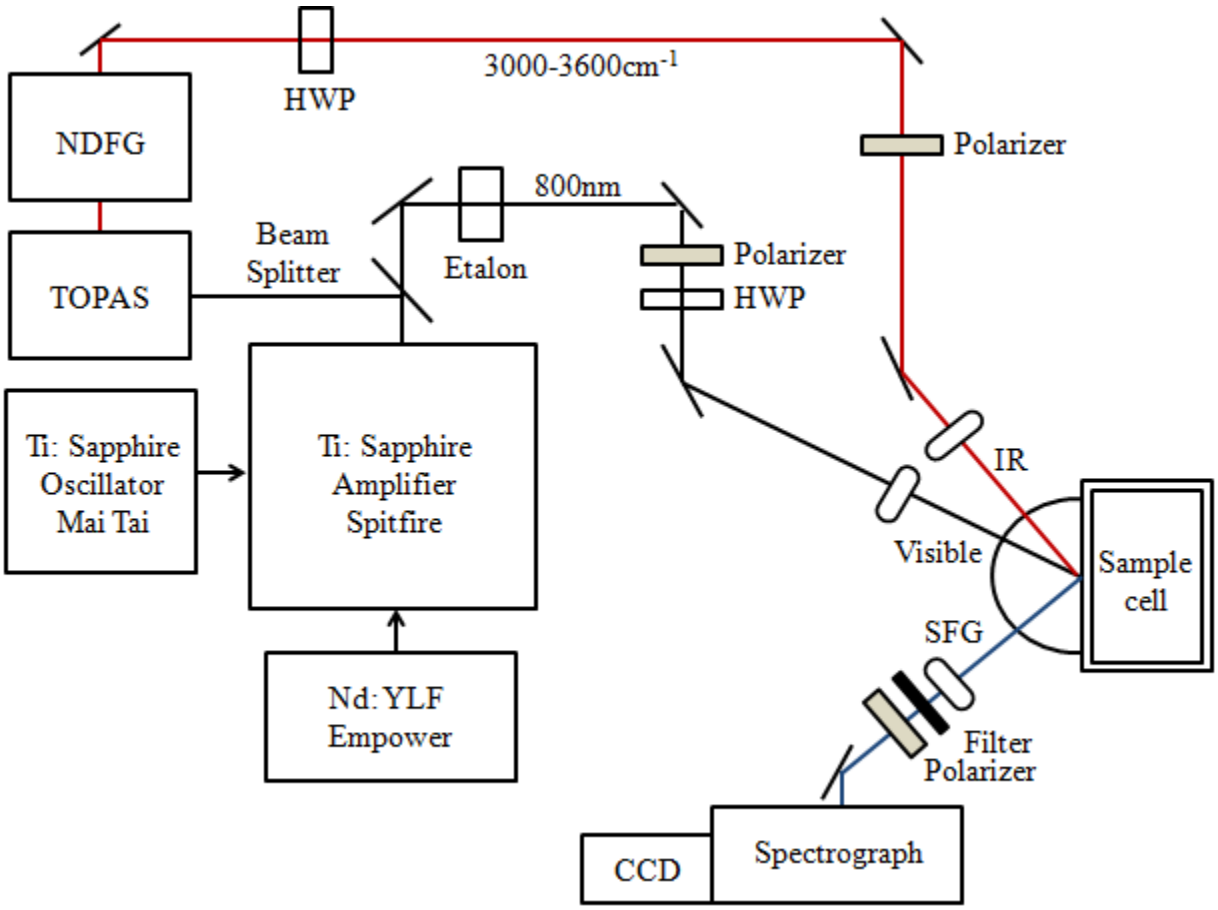

Figure 3.3. Schematic diagram of SFG laser system.

3.3.3. Preparation of Silica Surface.

The IR grade silica hemispheres were obtained from Almaz Optics, NJ, USA. Prior to use, the hemisphere was cleaned by sonicating it in Milli-Q water (5 min), then in methanol (5 min) and finally in water (5 min) again, with copious rinses of Milli-Q water (about 500 mL of water) in between sonications. The hemisphere was then covered with Piranha solution (3:1 mixture of H_2SO_4 and 30% H_2O_2) for an hour followed by a thorough washing with Milli-Q water. The hemisphere was then sonicated in water for 5 minutes for a total of three times, with rinses of Milli-Q water (about 1L of water) in between sonications. The cleaned hemisphere was then dried under the oven for about 30 minutes and plasma cleaned for 1-2 minutes until it was used

for experiments. For SFG experiments, another hemisphere was cleaned in the same way as described above and coated with gold (thickness of 200 nm) through chemical vapor deposition and used as a standard reference in the experiment for data normalization.

3.3.4. Preparation of Salt Solutions.

Salt solutions (0.1 M) were prepared by dissolving salts in ultrapure deionized water (18.2 MΩ·cm, MilliQ-Plus ultrapure water purification system, Millipore). All the solutions were prepared by using the inorganic salts as purchased and without any further purification. The pH of the solution was adjusted using the hydrochloric acid (trace metal grade, Fisher Scientific) solutions. The pH of all the solutions were measured with an Orion Versa Star, Star A, and Dual Star meters from Thermo Scientific (Orion, 8157UWMMD).

3.3.5. Materials.

High purity salts, and acids were selected for preparation of the salt solutions: NaCl (≥99.5%, Sigma-Aldrich), $NaHCO_3$ (≥99%, Caledon Laboratories Ltd.), and HCl (trace metal grade, Fisher Scientific). All materials were used without further purification. Ultrapure deionized water (18.2 MΩ) was used after deionization from a Milli-Q-Plus ultrapure water purification system (Millipore). All experiments were performed with freshly prepared solutions.

3.3.6. SHG pH Variation Experiments.

First, the sample cell was filled with Milli-Q water and the SHG signal was optimized. Next, the water in the sample cell was replaced by ~15 mL of the salt solution of interest that had been pH adjusted to around 8. This silica/aqueous interface was allowed to equilibrate for about 30 minutes while monitoring the SHG signal. After this equilibration time, aliquots of diluted hydrochloric acid in a solution of the same salt concentration (0.1 M) were added to adjust the

pH by ~0.3 pH units. At each new pH, the system was allowed to stand for ~3 min to reach equilibrium, and then SHG was collected for ~2 minutes. This step of changing the pH and measuring the corresponding SHG signal was repeated until the pH of the solution reached around 2.

3.3.7. SFG pH Variation Experiments.

Six reference SFG spectra were collected from a gold-coated IR grade silica surface from 3000 to 3500 cm^{-1}, which covered the OH stretching region of the water spectrum. The SFG spectra were acquired at five different settings of the incident IR wavelength such that the IR was centered at ~3000, 3100, 3200, 3300, 3400 and 3500 cm^{-1}. The SFG spectra were collected using the ssp (s-polarized SFG output, s-polarized visible input, and p-polarized IR input) or pss polarization combination (p-polarized SFG output, s-polarized visible input, and s-polarized IR input). After SFG spectra of the reference gold-coated silica had been collected, the gold-coated hemisphere was replaced a freshly cleaned IR grade silica hemisphere and aligned using irises to make sure the reflected light from the silica/water interface had the same alignment as the beam reflected from the gold-coated silica surface. For a given pH, six spectra with the central wavenumbers of ~3000, 3100, 3200, 3300, 3400 and 3500 cm^{-1} were measured for the silica/water interface in the same way as the gold-coated silica. The six spectra were then summed to generate a single spectrum covering the broad water spectrum. The summed water spectrum was then normalized by dividing by the sum of the six gold reference spectra to obtain a final, gold-normalized spectrum of interfacial water.[39-40] For all SFG measurements, a freshly cleaned fused silica hemisphere (Almaz optics, 1 inch diameter, IR-grade SiO_2) was placed on a custom-built Teflon cell so that the flat surface of the hemisphere was in contact with the aqueous phase. The top of the sample cell is exposed so that the salt solution could replace the

water and pH of the sample solution can be routinely changed and monitored from the top opening. SFG was first measured for the silica/water interface with the Milli-Q water as described above. The Milli-Q water was then replaced with ~15 mL of the salt solution which was adjusted to around pH~ 8 and was equilibrated for 30 min. After the equilibration time, six spectra were collected. Aliquots of the diluted hydrochloric acid which had same salt concentration (0.1 M) of the sample were added to adjust the pH by ~0.5 pH unit in the sample. After adding each aliquot, the solution was mixed by repeatedly removing and redispensing the solution with a glass pipette with a rubber bulb. At each new pH, the system was allowed to stand for ~3 min to reach equilibrium before the SFG spectrum was collected. pH was adjusted until pH of the solution reached around 5.

3.4. Results and Discussion

The Gouy-Chapman-Stern-Grahame (GCSG) model, which was used to describe specific cation effects in Chapter 2 was also used in this chapter to study the effect of HCO_3^- at silica/water interface and determine how the water structuring properties of bicarbonate influence its adsorption behaviours and the acid/base chemistry of silica.

3.4.1. SFG Results

In this work, vibrational SFG spectroscopy was used to monitor effect of HCO_3^- on the water structure at the silica/water interface. Specifically, the SFG of silica in the presence of 0.1 M $NaHCO_3$ or 0.1 M NaCl was measured from pH~ 8-5 and compared to determine the effect of HCO_3^-. Our group's previous study suggested that the two peaks observed in SFG spectra for the ssp polarization arise from two different water populations at the silica/water interface: one

coming from the alignment of water molecules within the Stern layer (~3400 cm^{-1}) and another one coming from the alignment of water molecules in diffuse layer (~3200 cm^{-1}).[47] Our group's previous research also suggested that the ssp-polarized SFG spectra is dominated by the 3200 cm^{-1} peak, corresponding to water molecules mostly in the diffuse layer, whereas the pss-polarized SFG spectra were dominated by the 3400 cm^{-1} peak corresponding to water molecules in Stern layer.[47] Therefore, we monitored the two different polarization combinations to determine how the net ordering of interfacial water molecules changes for the two water populations in Stern layer and diffuse layer at silica/water interface under different environmental conditions i.e. pH and the type of anion in solution.

Figure 3.4 and Figure 3.5 shows representative SFG spectra collected from silica/water interface at ssp and pss polarization combinations, respectively, in the presence of 0.1 M $NaHCO_3$ and 0.1 M NaCl. Firstly, the results show that the SFG intensity drops when salt has been added. This decrease in the net alignment of interfacial water is due to Na^+ screening the negative surface charge of silica which decreases the magnitude of the potential at both the inner Helmholtz plane, IHP (Φ_{IHP}) and the outer Helmholtz plane, OHP (Φ_{OHP}). In addition, the results also show that the SFG intensity generally decreases with decreasing pH in the presence of both $NaHCO_3$ and NaCl for both the ssp and pss polarization combinations. More specifically, a trend is also observed where the SFG intensity increases slightly from pH~ 8 to pH~ 7.5 and then decreases from pH~ 7.5 to pH~ 5 for both salts for both ssp and pss polarization combinations.

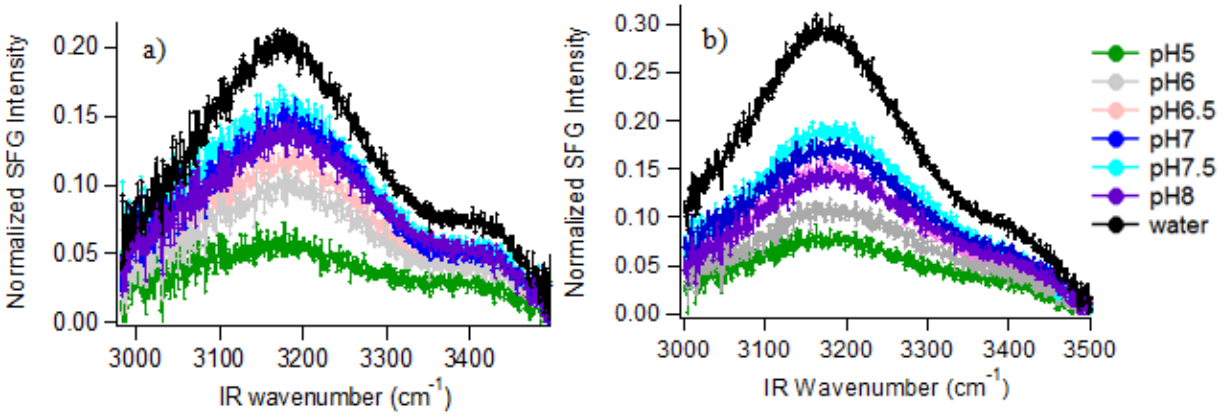

Figure 3.4. Representative figure of SFG of a) 0.1 M $NaHCO_3$ and b) 0.1 M NaCl at ssp polarization.

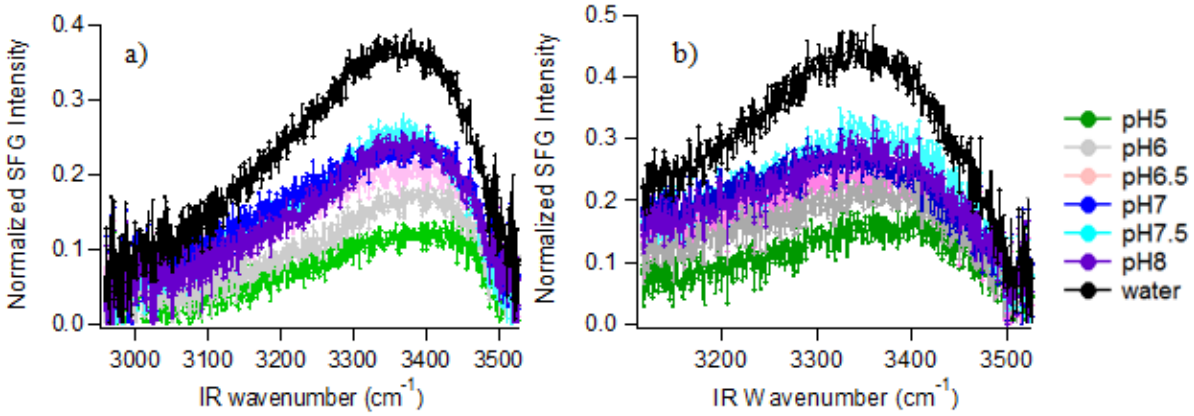

Figure 3.5. Representative figure of SFG of a) 0.1 M $NaHCO_3$ and b) 0.1 M NaCl at pss polarization.

The changes in the SFG intensity under varied pH are difficult to compare between $NaHCO_3$ and NaCl by looking at the SFG spectra alone. Therefore, to determine if these changes in SFG intensity are specific to HCO_3^-, the SFG spectra was integrated between 3000-3450 cm^{-1}

and then divided by the integrated SFG intensity of water that was collected at the beginning of each experiment to observe how the mean SFG intensity changed as a function of pH for both salts. If $NaHCO_3$ is present in or near the Stern layer, there will be greater negative charge near the surface and therefore the SFG intensity of $NaHCO_3$ should be greater than NaCl for the ssp polarization combination. In case of NaCl, Cl^- ions are likely staying further away from the surface than HCO_3^- , and consequently less charge is present.[98] Figure 3.6 shows the water normalized mean integrated SFG intensity for 0.1 M $NaHCO_3$ and 0.1 M NaCl. From the integration results, we observe that the water normalized mean integrated SFG intensity for $NaHCO_3$ is higher than that of NaCl under ssp polarization combination. On the other hand, the water normalized mean integrated SFG intensity of $NaHCO_3$ and NaCl looked similar for the pss polarization combination. The fact that specific anion effects are observed only for the ssp and not the pss-SFG indicates that HCO_3^- is present at or near the outer Helmholtz plane, counteracting the positive charge of the sodium present at the outer Helmholtz plane leading to a larger magnitude of the outer Helmholtz potential than in the presence of chloride (Figure 3.7). Halide effects studied by Azam et al. at the silica/aqueous interface suggested that ions such as iodide, which has water breaking properties become partially desolvated, and partition to the silica/aqueous interface which has a compact layer consisting of stabilizing clusters of siloxide-Na^+ complexes.[39] Likewise, bicarbonate anions may have water structure breaking properties and may become partially desolvated and partition to the silica/aqueous interface, yet still residing far enough from the surface to not alter the adjacent water structure. Furthermore, it is possible that bicarbonate may be attracted to surface layer species, which possibly consist of siloxide-Na^+ complexes.

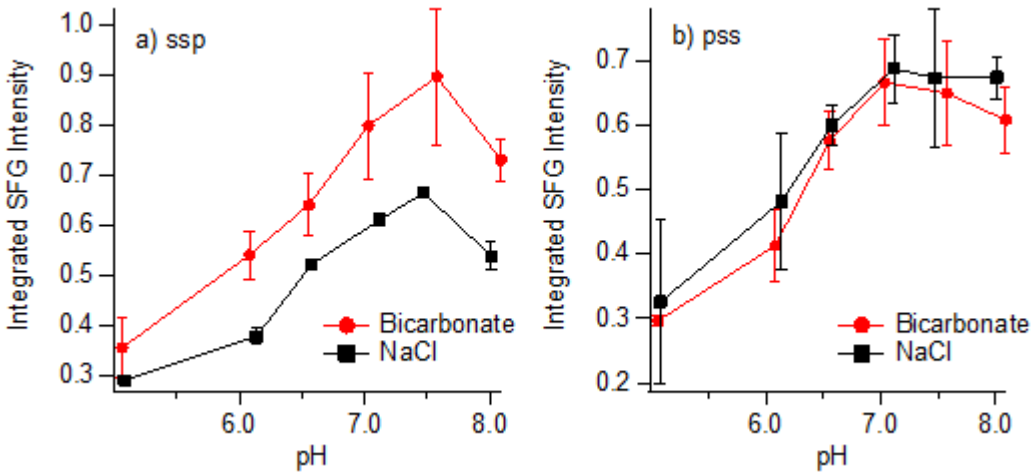

Figure 3.6. Water normalized mean integrated intensity of SFG for 0.1 M $NaHCO_3$ and 0.1 M NaCl at a) ssp polarization b) pss polarization.

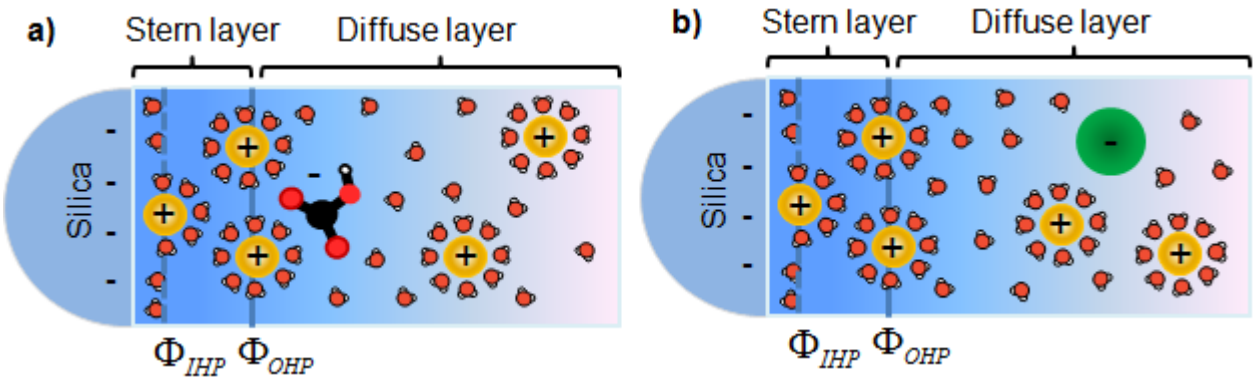

Figure 3.7. Schematic of a) bicarbonate anion positioned closer to the silica/aqueous interface and b) chloride anion positioned further away from the silica/aqueous interface.

In addition, when we plot the water normalized integrated intensity of SFG as a function of pH for both salts, we observe a hump near pH 7.5 as shown in Figure 3.6. In general, if silica is getting more negatively charged with increasing pH, then there should be more alignment of water molecules at the interface due to the charge at the interface and an increase in the SFG

intensity. Yet, for both $NaHCO_3$ and NaCl, the intensity of SFG increased from pH~ 5 to pH~ 7.5 and then decreased from pH~ 7.5 to pH~ 8.0. This decrease with increasing pH is likely not due to HCO_3^- because it was observed for both $NaHCO_3$ and NaCl solutions. The hump at pH~ 7.5 could be evidence of hysteresis as such a hump has not been observed in titrations initiated at pH 6 with increasing pH. Instead, only these titrations started from pH 8 and decreasing in pH revealed such a feature.[38-40, 47, 49] Such hysteresis was discussed in Darlington et al., where the authors revealed starting SHG titrations at pH~ 12.0, 2.0, 6.0, or 7.0, yielded different distributions of three unique silanol sites.[49] The hump could be due to changes in surface acidity. It could also indicate changes in the Stern layer structure like a transition from specific adsorption of sodium at pH 8 (at the inner Helmholtz plane) to non-specific adsorption at pH 7.5 (at the outer Helmholtz plane), which could lead to the observed changes in the outer Helmholtz potential. To more accurately assess the influence of bicarbonate and chloride as well as varying pH on the two different water populations, peak fitting was performed for two peaks (~3200 cm^{-1} and ~3400 cm^{-1}) on SFG spectra for ssp polarization combination. Each SFG spectra was fitted to the absolute square of summed Lorentzian functions.[1] The average of A/Γ values from multiple fitting results was calculated and was plotted at varying pH with error bars representing standard deviation (±Sd) (Figure 3.8). A is the peak amplitude and Γ is a parameter describing the line width (full width at half maximum, FWHM) of the Lorentzian functions. Results for peak fitting of the 3200 cm^{-1} and 3400 cm^{-1} peaks are shown in Figure 3.8. Peak fitting results for the ~3200 cm^{-1} peak agrees with the integrated ssp-SFG intensity results. The peak amplitudes at ~3200 cm^{-1} peak for $NaHCO_3$ is greater than NaCl suggesting that more HCO_3^- is present at or near the outer Helmholtz plane than for chloride. The standard deviation was too large for the ~3400 cm^{-1} peak to draw any conclusions from the fitting results.

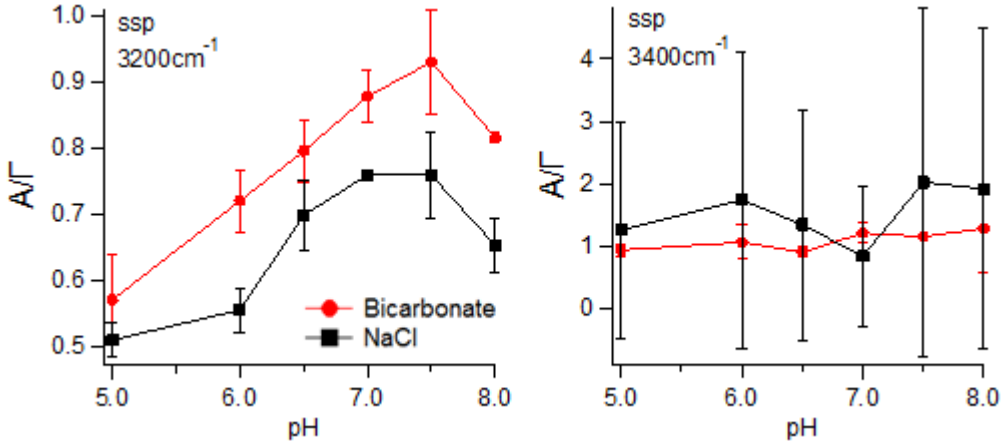

Figure 3.8. Representative peak fitting results for ssp SFG water spectra in the presence of 0.1 M $NaHCO_3$ and NaCl as a function of pH. A/Γ for the 3200 cm^{-1} peak is shown in a) and A/Γ for the peak at ~3400 cm^{-1} are shown in b).

To summarize this SFG section, the increase in the overall intensity of SFG in the presence of bicarbonate compared with chloride in the ssp-SFG appears to arise not from the adsorption of sodium bicarbonate to the silica/aqueous interface but rather due to bicarbonate ions partitioning towards the Stern layer that includes the sodium counterions. Moreover, the hump occurring at pH~ 7.5 shown in Figure 3.7 is possibly due to hysteresis. SHG techniques were used to further investigate the hump and determine if the hump is due to the changes in the ordering of the interfacial water molecules which is induced by the changes in the interfacial potential or due to changes in the surface sites of silica.

3.4.2. SHG Results

As shown in Chapter 1, the intensity of SHG is proportional to the interfacial potential term. Moreover, the surface charge density of silica is directly proportional to the interfacial

potential under high salt concentration ($\geq$0.1 M) according to the constant capacitance model.[46] Thus, at high salt concentration, any SHG intensity changes should be directly related to the changes in the surface potential of silica. The Na^+ cation was kept constant for all experiments and only the anion was varied to specifically look at bicarbonate anion effects. Previous SFG results suggest that new silica sites may be forming at pH~ 7.5 due to hysteresis effects from different starting pH conditions. The integrated SFG results showed that there is a hump near pH~ 7.5. The SHG results, on the other hand, exhibit a hump near pH 6.5 as shown in Figure 3.9. The differences in the pH at where the hump is occurring could be because SHG formally includes responses from the silica surface as well as net aligned water, whereas SFG only selectively probes the OH stretches.[48] In addition to the hump, we observe that the overall water normalized integrated SHG intensity for NaCl is greater than $NaHCO_3$, which was the opposite trend observed with SFG. When we add NaCl solution, the SHG intensity should decrease more than $NaHCO_3$ due to greater screening of sodium cations. Here, we see that the water normalized integrated SHG intensity is higher for NaCl than $NaHCO_3$ salts. More SHG experiments would need to be performed to determine the cause for this phenomenon. Nonetheless, in both SHG and SFG titrations starting at pH~ 8.0, hysteresis effects are observed where there is possible formation of mid acidic silica surface sites which are kinetically trapped structures rather than the thermodynamic minimum of the surface for both 0.1 M $NaHCO_3$ and 0.1 M NaCl. From pH~ 7.0 to pH~ 8.0, the SHG intensity increases due to the silica surface becoming more negative and also causing more alignment of interfacial water molecules.

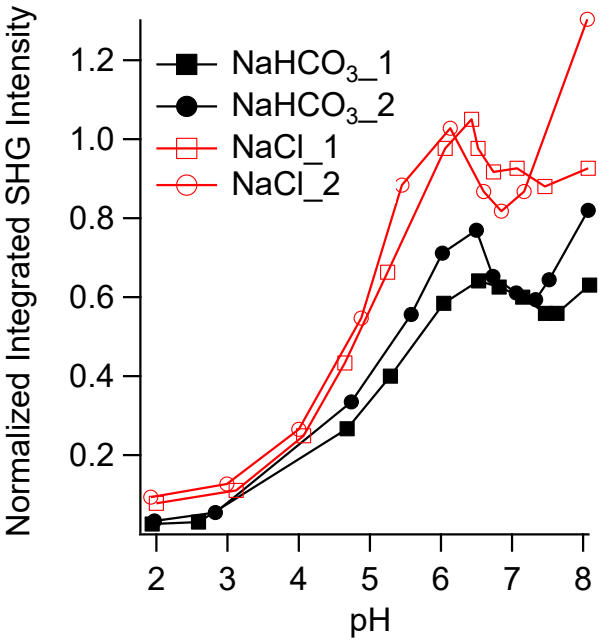

Figure 3.9. Water normalized integrated SHG intensity of 0.1 M $NaHCO_3$ and 0.1 M NaCl solution at the silica/aqueous interface.

3.5. Conclusion

Based on our SFG and SHG results, we can conclude that HCO_3^- is a good dispersant for silica, not because it binds directly to the silica surface but rather because HCO_3^- partitions towards the Stern layer and reduces the screening of the Na^+ cations felt in the diffuse layer thereby increasing the magnitude of the potential felt by the local waters. Consistent with weaker water structuring properties, the partitioning of HCO_3^- towards the interface appears to be greater than for Cl^-. Furthermore, hysteresis effects were observed as a result of starting from slightly basic conditions. SFG and SHG results show that upon a starting pH of 8.0, we may be observing kinetically trapped mid acidic silica surface sites which have siloxide groups donating hydrogen bonds to interfacial water molecules and has a pK_a of ~5.2. The pKa of these mid-acidic sites

was found to be different between the two techniques, possibly indicating fundamental differences in the two measurements. One possible explanation, is that as SHG is non-resonant its signal intensity could also include large contributions from the silica surface sites ($\chi^{(2)}_{silica}$) whereas SFG is resonant for OH stretches and more specifically probes OH stretches which comes from the interfacial water molecules. More SHG experiments need to be done to further investigate the hysteresis effects on the acid-base chemistry of silica. Future titrations could be performed at longer time to determine whether the silica surface would establish equilibrium with longer time to avoid hysteresis and also determine the equilibration time if it is indeed hysteresis that changed the silica surface. We would also like to probe C=O carbonyl stretches using the SFG for both ssp and pss polarization to specifically look at bicarbonate ions and confirm that bicarbonate ions are indeed present within the diffuse layer of electrical double layer of the silica/aqueous interface.

Chapter 4

General conclusion and future work

4.1. General Conclusion

In this thesis, nonlinear optical techniques SHG and SFG were used to study how different ions affect the acid-base chemistry of silica and also the ordering of interfacial water molecules at the silica/aqueous interface. Our work can be used to study the silica/aqueous interface occurring in many geological, environmental and industrial processes at a molecular level. It can be used in applications such as environmental modelling for controlling different pollutant adsorption to silica in silica reservoirs of natural water and oil as well as improving the efficiency of separation of bitumen from oil sands and the densification of oil sands tailings.

In Chapter 2, SFG was used to probe the OH stretching region of water to investigate the effect of monovalent cations (0.1 M Li^+, Na^+, K^+, Cs^+) on the water structure at the electrical double layer (EDL) of the silica/aqueous interface. Cl^- was kept the same for all four salts to focus on the specific cation effects. SFG results showed that specific cation effects are dependent on the pH of the solution as we observed a reverse trend in the affinity of the ion to silica surface from near-neutral pH to high pH. The SFG intensity for Cs^+ was greatest above pH~ 10 and we attributed this to expulsion of Cs^+ from the silica surface due to stronger electrostatic interaction between interfacial water molecules and the silica surface. At pH~ 7-10, Cs^+ has the lowest SFG intensity at 3200 cm^{-1} as silica becomes less negative and causes chaotropic Cs^+ to accumulate near the surface due to hydrophobic interactions. Below pH 7, the SFG peak at 3200 cm^{-1} began to increase for all four of the electrolytes studied as the pH was lowered to 2, which was attributed to a combination of overcharging of the EDL and ordering of water molecules in the cation hydration layer. Greater adsorption of Cs^+ occurred than Li^+. Overall, we observed different ordering of interfacial water molecules for each of the water populations at the silica/aqueous interface depending on the ion size and hydration shell of cation and these

observed specific cation effects were shown to be dependent on the pH of the solution. Overall, we were able to use SFG to determine the amount of perturbation of interfacial water structure at the silica/aqueous interface and gain fundamental understanding of how specific ions and its water structure making/breaking properties influence the $\Phi_{0,}$ Φ_{OH}, thickness of the Stern layer as well as the affinity of the ion for silica. We were also able to show that trends in the SFG spectra shapes and intensities that are influenced by these properties of $\Phi_{0,}$ Φ_{OH}, thickness of the Stern layer, and the ion affinity are dependent on the pH of the solution. Our findings are meaningful for better understanding of the structure of the electric double layer (EDL) occurring at silica/aqueous interface as we have shown that the capacitance of the electric double layer (EDL) is not constant but is dependent on the type of the salt and the pH of the solution.

In Chapter 3, SFG and SHG was used to investigate the effect of bicarbonate ion and chloride ion (0.1 M Cl^- and HCO_3^-) on the water structure and the acid-base chemistry of the silica/aqueous interface. NaCl was measured as a reference and was compared with 0.1 M $NaHCO_3$ to keep the Na^+ cation the same and investigate how introducing HCO_3^- would affect the silica/aqueous interface. We have also obtained the SFG spectra for ssp and pss polarization combinations to study two different water populations (water in the Stern layer which is dominated by pss-SFG spectra as well as 3400 cm^{-1} peak in ssp-SFG spectra and water in the diffuse layer dominated by 3200 cm^{-1} peak in ssp-SFG spectra). The SFG results showed that for ssp polarization combination, the intensity of SFG for HCO_3^- was greater than Cl^- from pH~ 5 to pH~ 8 whereas for pss polarization combination, the intensity of SFG did not vary greatly between the two salts. These results suggest that the bicarbonate anions may be partitioned to Na^+ coordinated siloxide surface and increase the SFG intensity and we may be detecting OH stretches coming from the bicarbonate anion in diffuse layer. The similarity in trends in pss SFG

was attributed to similarities in Stern layer structure, with contributions largely arising from water molecules and Na^+ ions within Stern layer for both salts. Overall, our work showed the bicarbonate anion effects at the silica/aqueous interface which has never been observed using SFG. Bicarbonate is known to act as a dispersant compared to chloride ion for silica colloids and we observe an increase in I_{SFG} at ~3200 cm^{-1} in ssp-SFG spectra when we introduce bicarbonate to the solution. From this, we can speculate that greater I_{SFG} correlates with better dispersion properties of an ion. Accordingly, we can now screen different additives and monitor the performance of the additives in silica colloids using SFG which could be applied in developing a method for improving the efficiency of the dewatering of oil sands tailings as well as improving the separation of oil sands during bitumen extraction process.

4.2. Future Work

In this thesis, we have largely focused on pH-dependent cation specific effects on the ordering of interfacial water molecules at silica/aqueous interface. For future work, the effect of halide ions can be studied using SFG and the SFG spectra of 0.5 M NaCl, NaBr, NaI can be measured to further investigate the effect of anions at silica/aqueous interface. Since bromide and iodide ion is more chaotropic than chloride ion, we would expect bromide and iodide to adsorb to silica surface under low pH and observe different specific ion effects under presence of bromide or chloride ion as opposed to chloride ion. In addition, we would like to measure both zeta potential and the SFG of silica under different dewatering agents such as gypsum ($CaSO_4$) and compare the results to confirm that the SFG intensity is associated with the dispersing properties of an ion in colloidal silica. Dewatering agents such as gympsum should have less

water molecules at the silica/aqueous interface and we would expect to observe very little SFG intensity in the SFG spectra.

In addition, we have also looked at how 0.1 M $NaHCO_3$ and NaCl affect the acid-base chemistry of silica/aqueous interface. In addition, our current SFG measurements for $NaHCO_3$ suggest that we are probing OH stretches which come from both water and bicarbonate anion. To distinguish contributions from the two species, C=O stretching regions that can only arise from HCO_3^- will be probed using SFG technique to confirm the presence of HCO_3^- in diffuse layer at silica/aqueous interface. We would expect to see an increase in C=O stretching regions coming from the HCO_3^- anion for ssp polarization combination and observe very little signal for pss polarization combination if the HCO_3^- anion is located in the diffuse layer. Zeta potential measurements could also be performed for both $NaHCO_3$ and NaCl with a starting pH~ 8 to determine if similar hump is observed near pH~ 7.5 (which would be similar to SFG results) or near pH~ 6.5 (similar to SHG results) regions. If HCO_3^- is indeed present within the diffuse layer, we should be able to see the difference in the magnitude of zeta potential of silica between $NaHCO_3$ and NaCl solution. It would also be interesting to see if we can observe hysteresis effects and changes in the silica surface sites through zeta potential measurements. Lastly, titrations can be performed using SFG under a closed system where no CO_2 can be dissolved in air to ensure that we do not have any formation of bicarbonate in the solution due to CO_2 dissolved in aqueous solution.

References

1. Shen, Y. R.; Ostroverkhov, V., Sum-Frequency Vibrational Spectroscopy on Water Interfaces: Polar Orientation of Water Molecules at Interfaces. *Chem. Rev.* **2006,** *106*, 1140-1154.

2. Dove, P. M.; Rimstidt, J. D., Silica-Water Interactions. In *Reviews in Mineralogy Series: The Silica Polymorphs*, Heaney, P.; Prewitt, C.; Gibbs, G., Eds. Mineralogical Society of America: 1994; Vol. 29, pp 259-308.

3. Kosmulski, M., pH-dependent surface charging and points of zero charge. IV. Update and new approach. *J. Coll. Interf. Sci.* **2009,** *337* (2), 439-448.

4. Masliyah, J.; Zhou, Z. J.; Xu, Z.; Czarnecki, J.; Hamza, H., Understanding Water-Based Bitumen Extraction from Athabasca Oil Sands. *Can. J. Chem. Eng.* **2004,** *82* (4), 628-654.

5. Zhao, H.; Dang-Vu, T.; Long, J.; Xu, Z.; Masliyah, J. H., Role of Bicarbonate Ions in Oil Sands Extraction Systems with a Poor Processing Ore. *J. Dispersion Sci. Technol.* **2009,** *30* (6), 809-822.

6. Hall, E. S.; Tollefson, E. L., Stabilization and destabilization of mineral fines-bitumen-water dispersions in tailings from oil sand extraction plants that use the hot water process. *Can. J. Chem. Eng.* **1982,** *60* (6), 812-821.

7. Brady, P. V.; Walther, J. V., Kinetics of quartz dissolution at low temperatures. *Chem. Geol.* **1990,** *82*, 253-264.

8. Dove, P.; Craven, C., Surface charge density on silica in alkali and alkaline earth chloride electrolyte solutions. *Geochim. Cosmochim. Acta* **2005,** *69* (21), 4963-4970.

9. Brown, M. A. G., A.; Abbas, Z., Effect of Electrolyte Concentration on the Stern Layer Thickness at a Charged Interface. *Angew. Chem. Int. Ed.* **2016,** *55* (11), 3790-3794.

10. Davis, J. A.; James, R. O.; Leckie, J. O., Surface Ionization and Complexation at the Oxide/Water InterfaceL I. Computation of Electrical Double Layer Properties in Simple Electrolytes. *J. Coll. Interf. Sci.* **1978,** *63* (3), 480-499.

11. Grahame, D. C., The Electrical Double Layer and the Theory of Electrocapillarity. *Chem. Rev.* **1947,** *41* (3), 441-501.

12. Kitamura, A.; Fujiwara, K.; Yamamoto, T.; Nishikawa, S.; Moriyama, H., Analysis of Adsorption Behavior of Cations onto Quartz Surface by Electrical Double-layer Model. *J. Nucl. Sci. Technol.* **1999,** *36*, 1167-1175.

13. Parsons, R., The electrical double layer: recent experimental and theoretical developments. *Chem. Rev.* **1990,** *90* (5), 813-826.

14. Torrie, G. M.; Kusalik, P. G.; Patey, G. N., Theory of the electrical double layer: Ion size effects in a molecular solvent. *J. Chem. Phys.* **1989,** *91* (10), 6367-6375.

15. Tournassat, C.; Chapron, Y.; Leroy, P.; Bizi, M.; Boulahya, F., Comparison of molecular dynamics simulations with triple layer and modified Gouy–Chapman models in a 0.1 M NaCl–montmorillonite system. *J. Coll. Interf. Sci.* **2009,** *339* (2), 533-541.

16. Hsu, W. L. D., H.; Dunstan, D.E.; Davidson, M. R.; Harvie, D. J. E., Electrokinetics of the silica and aqueous electrolyte solution interface: Viscoelectric effects. *Adv. Colloid Interface Sci.* **2016,** *234*, 108-131.

17. Cacace, M. G.; Landau, E. M.; Ramsden, J. J., The Hofmeister series : salt and solvent effects on interfacial phenomena. *Quart. Rev. Biophys.* **1997,** *30* (3), 241-277.

18. Collins, K. D.; Washabaugh, M. W., The Hofmeister effect and the behaviour of water at interfaces. *Quart. Rev. Biophys.* **1985,** *18* (4), 323-422.

19. Morag, J.; Dishon, M.; Sivan, U., The Governing Role of Surface Hydration in Ion Specific Adsorption to Silica: An AFM-Based Account of the Hofmeister Universality and Its Reversal. *Langmuir* **2013,** *29* (21), 6317-6322.

20. Parsons, D. F.; BostroÃàm, M.; Maceina, T. J.; Salis, A.; Ninham, B. W., Why Direct or Reversed Hofmeister Series? Interplay of Hydration, Non-electrostatic Potentials, and Ion Size. *Langmuir* **2009,** *26* (5), 3323-3328.

21. Parsons, D. F.; Bostrom, M.; Nostro, P. L.; Ninham, B. W., Hofmeister effects: interplay of hydration, nonelectrostatic potentials, and ion size. *Phys. Chem. Chem. Phys.* **2011,** *13* (27), 12352-12367.

22. Xie, W.; Liu, C.; Yang, L.; Gao, Y., On the molecular mechanism of ion specific Hofmeister series. *Sci. China Chem.* **2014,** *57* (1), 36-47.

23. Zhang, Y.; Cremer, P., Interactions between macromolecules and ions: the Hofmeister series. *Curr. Opin. Chem. Biol.* **2006,** *10* (6), 658-663.

24. Chen, X.; Flores, S. C.; Lim, S.-M.; Zhang, Y.; Yang, T.; Kherb, J.; Cremer, P. S., Specific Anion Effects on Water Structure Adjacent to Protein Monolayers. *Langmuir* **2010,** *26*, 16447-16454.

25. Paterová, J.; Rembert, K. B.; Heyda, J.; Kurra, Y.; Okur, H. I.; Liu, W. R.; Hilty, C.; Cremer, P. S.; Jungwirth, P., Reversal of the Hofmeister Series: Specific Ion Effects on Peptides. *J. Phys. Chem. B* **2013,** *117* (27), 8150-8158.

26. Collins, K. D.; Neilson, G. W.; Enderby, J. E., Ions in water: Characterizing the forces that control chemical processes and biological structure. *Biophys. Chem.* **2007,** *128* (2-3), 95-104.

27. Baldwin, R. L., How Hofmeister ion interactions affect protein stability. *Biophys. J.* **1996,** *71* (4), 2056-2063.

28. Salis, A.; Ninham, B. W., Models and mechanisms of Hofmeister effects in electrolyte solutions, and colloid and protein systems revisited. *Chem. Soc. Rev.* **2014,** *43* (21), 7358-7377.

29. Schwierz, N.; Horinek, D.; Netz, R. R., Reversed Anionic Hofmeister Series: The Interplay of Surface Charge and Surface Polarity. *Langmuir* **2010,** *26* (10), 7370-7379.

30. Salis, A.; Bhattacharyya, M. S.; Monduzzi, M., Specific Ion Effects on Adsorption of Lysozyme on Functionalized SBA-15 Mesoporous Silica. *J. Phys. Chem. B* **2010,** *114* (23), 7996-8001.

31. Chen, X.; Yang, T.; Kataoka, S.; Cremer, P. S., Specific Ion Effects on Interfacial Water Structure near Macromolecules. *J. Am. Chem. Soc.* **2007,** *129* (40), 12272-12279.

32. Flores, S. C. K., J.; Cremer, P.S., Direct and Reverse Hofmeister Effects on Interfacial Water Structure. *J. Phys. Chem. C* **2012,** *116*, 14408−14413.

33. Flores, S. C.; Kherb, J.; Konelick, N.; Chen, X.; Cremer, P. S., The Effects of Hofmeister Cations at Negatively Charged Hydrophilic Surfaces. *J. Phys. Chem. C* **2012,** *116* (9), 5730-5734.

34. Brown, M. A.; Abbas, Z.; Kleibert, A.; Green, R. G.; Goel, A.; May, S.; Squires, T. M., Determination of Surface Potential and Electrical Double-Layer Structure at the Aqueous Electrolyte-Nanoparticle Interface. *Phys. Rev. X* **2016,** *6* (1), 011007.

35. Schwierz, N.; Horinek, D.; Netz, R. R., Anionic and Cationic Hofmeister Effects on Hydrophobic and Hydrophilic Surfaces. *Langmuir* **2013,** *29* (8), 2602-2614.

36. Dishon, M.; Zohar, O.; Sivan, U., From Repulsion to Attraction and Back to Repulsion: The Effect of NaCl, KCl, and CsCl on the Force between Silica Surfaces in Aqueous Solution. *Langmuir* **2009,** *25*, 2831-2836.

37. Hribar, B.; Southall, N. T.; Vlachy, V.; Dill, K. A., How Ions Affect the Structure of Water. *J. Am. Chem. Soc.* **2002,** *124* (41), 12302-12311.

38. Azam, M. S.; Weeraman, C. N.; Gibbs-Davis, J. M., Specific Cation Effects on the Bimodal Acid–Base Behavior of the Silica/Water Interface. *J. Phys. Chem. Lett.* **2012,** *3* (10), 1269-1274.

39. Azam, M. S.; Weeraman, C. N.; Gibbs-Davis, J. M., Halide-Induced Cooperative Acid–Base Behavior at a Negatively Charged Interface. *J. Phys. Chem. C* **2013,** *117* (17), 8840-8850.

40. Md Shafiul, A.; Akemi, D.; Julianne, M. G.-D., The influence of concentration on specific ion effects at the silica/water interface. *J. Phys. Condens. Matter* **2014,** *26* (24), 244107.

41. Boyd, R. W., *Nonlinear Optics Third Edition*. Academic Press: Rochester, New York, 2007.

42. Sutherland, R. L. M., D. G.; Kirkpatrick, S., *Handbook of Nonlinear Optics, 2nd Ed.* Marcel Dekker: New York, 2003.

43. Baxter, G. P.; Burgess, L. L.; Daudt, H. W., THE REFRACTIVE INDEX OF WATER. *J. Am. Chem. Soc.* **1911,** *33* (6), 893-901.

44. Khlebtsov, B. N.; Khanadeev, V. A.; Khlebtsov, N. G., Determination of the Size, Concentration, and Refractive Index of Silica Nanoparticles from Turbidity Spectra. *Langmuir* **2008,** *24* (16), 8964-8970.

45. Paniagua-Domínguez, R.; Yu, Y. F.; Miroshnichenko, A. E.; Krivitsky, L. A.; Fu, Y. H.; Valuckas, V.; Gonzaga, L.; Toh, Y. T.; Kay, A. Y. S.; Luk'yanchuk, B.; Kuznetsov, A. I., Generalized Brewster effect in dielectric metasurfaces. *Nat. Commun.* **2016,** *7*, 10362.

46. Ong, S.; Zhao, X.; Eisenthal, K. B., Polarization of water molecules at a charged interface: second harmonic studies of the silica/water interface. *Chem. Phys. Lett.* **1992,** *191* (3,4), 327-335.

47. Darlington, A. M. J., T.; Kerian, E.; Roy, S.; Kim, S.; Azam, M.S.; Hore, D.K.; Gibbs, J.M., Separating the pH-Dependent Behavior of Water in the Stern and Diffuse Layers with Varying Salt Concentration. *J. Phys. Chem. C* **2017,** *In revision*.

48. Darlington, A. M. Studying the Effects of pH, Ion Concentration and Ion Valence on the Silica/Water Interface Using Nonlinear Optical Spectroscopy. University of Alberta, Edmonton, AB, 2016.

49. Darlington, A. M.; Gibbs-Davis, J. M., Bimodal or Trimodal? The Influence of Starting pH on Site Identity and Distribution at the Low Salt Aqueous/Silica Interface. *J. Phys. Chem. C* **2015,** *119* (29), 16560-16567.

50. Covert, P. A.; Jena, K. C.; Hore, D. K., Throwing Salt into the Mix: Altering Interfacial Water Structure by Electrolyte Addition. *J. Phys. Chem. Lett.* **2014,** *5*, 143-148.

51. Yang, Z.; Li, Q.; Chou, K. C., Structures of Water Molecules at the Interfaces of Aqueous Salt Solutions and Silica: Cation Effects. *J. Phys. Chem. C* **2009,** *113*, 8201–8205.

52. Jena, K. C.; Hore, D. K., Variation of Ionic Strength Reveals the Interfacial Water Structure at a Charged Mineral Surface. *J. Phys. Chem. C* **2009,** *113* (34), 15364-15372.

53. Mondal, J. A.; Nihonyanagi, S.; Yamaguchi, S.; Tahara, T., Structure and Orientation of Water at Charged Lipid Monolayer/Water Interfaces Probed by Heterodyne-Detected Vibrational Sum Frequency Generation Spectroscopy. *J. Am. Chem. Soc.* **2010,** *132* (31), 10656-10657.

54. Nihonyanagi, S.; Yamaguchi, S.; Tahara, T., Direct evidence for orientational flip-flop of water molecules at charged interfaces: A heterodyne-detected vibrational sum frequency generation study. *J. Chem. Phys.* **2009,** *130* (20), 204704-5.

55. Yamaguchi, S.; Tahara, T., Precise Electronic χ(2) Spectra of Molecules Adsorbed at an Interface Measured by Multiplex Sum Frequency Generation. *J. Phys. Chem. B* **2004,** *108* (50), 19079-19082.

56. Carrasco, J.; Hodgson, A.; Michaelides, A., A molecular perspective of water at metal interfaces. *Nat. Mater.* **2012,** *11* (8), 667-674.

57. Flores, S. C.; Kherb, J.; Konelick, N.; Chen, X.; Cremer, P. S., The Effects of Hofmeister Cations at Negatively Charged Hydrophilic Surfaces. *J. Phys. Chem. C* **2012,** *116*, 5730−5734.

58. Kim, J.; Cremer, P. S., IR−Visible SFG Investigations of Interfacial Water Structure upon Polyelectrolyte Adsorption at the Solid/Liquid Interface. *J. Am. Chem. Soc.* **2000,** *122* (49), 12371-12372.

59. Knauss, K. G.; Wolery, T. J., The dissolution kinetics of quartz as a function of pH and time at 70°C. *Geochim. Cosmochim. Acta* **1988,** *52* (1), 43-53.

60. Brady, P. V.; Walther, J. V., Controls on silicate dissolution rates in neutral and basic pH solutions at 25°C. *Geochim. Cosmochim. Acta* **1989,** *53* (11), 2823-2830.

61. Gratz, A. J.; Bird, P.; Quiro, G. B., Dissolution of quartz in aqueous basic solution, 106–236°C: Surface kinetics of "perfect" crystallographic faces. *Geochim. Cosmochim. Acta* **1990,** *54* (11), 2911-2922.

62. Wolff-Boenisch, D.; Gislason, S. R.; Oelkers, E. H.; Putnis, C. V., The dissolution rates of natural glasses as a function of their composition at pH 4 and 10.6, and temperatures from 25 to 74°C. *Geochim. Cosmochim. Acta* **2004,** *68* (23), 4843-4858.

63. Rimstidt, J. D.; Barnes, H. L., The kinetics of silica-water reactions. *Geochim. Cosmochim. Acta* **1980,** *44* (11), 1683-1699.

64. Mazer, J. J.; Walther, J. V., Dissolution kinetics of silica glass as a function of pH between 40 and 85°C. *J. Non-Cryst. Solids.* **1994,** *170* (1), 32-45.

65. Pham, A. L.-T.; Sedlak, D. L.; Doyle, F. M., Dissolution of mesoporous silica supports in aqueous solutions: Implications for mesoporous silica-based water treatment processes. *Appl. Catal. B* **2012,** *126*, 258-264.

66. Nangia, S.; Garrison, B. J., Reaction Rates and Dissolution Mechanisms of Quartz as a Function of pH. *J. Phys. Chem. A* **2008,** *112* (10), 2027-2033.

67. Gratz, A. J.; Bird, P., Quartz dissolution: Negative crystal experiments and a rate law. *Geochim. Cosmochim. Acta* **1993,** *57* (5), 965-976.

68. Dove, P. M.; Elston, S. F., Dissolution kinetics of quartz in sodium chloride solutions: Analysis of existing data and a rate model for 25°C. *Geochim. Cosmochim. Acta* **1992,** *56* (12), 4147-4156.

69. Dove, P. M.; Crerar, D. A., Kinetics of quartz dissolution in electrolyte solutions using a hydrothermal mixed flow reactor. *Geochim. Cosmochim. Acta* **1990,** *54* (4), 955-969.

70. Bennett, P. C., Quartz dissolution in organic-rich aqueous systems. *Geochim. Cosmochim. Acta.* **1991,** *55* (7), 1781-1797.

71. Dove, P. M., The dissolution kinetics of quartz in aqueous mixed cation solutions. *Geochim. Cosmochim. Acta* **1999,** *63* (22), 3715-3727.

72. Dewan, S.; Yeganeh, M. S.; Borguet, E., Experimental Correlation Between Interfacial Water Structure and Mineral Reactivity. *J. Phys. Chem. Lett.* **2013,** *4* (11), 1977-1982.

73. Al-Abadleh, H. A.; Mifflin, A. L.; Bertin, P. A.; Nguyen, S. T.; Geiger, F. M., Control of carboxylic acid and ester groups on chromium (VI) binding to functionalized silica/water interfaces studied by second harmonic generation. *J. Phys. Chem. B* **2005,** *109* (19), 9691-9702.

74. Al-Abadleh, H. A.; Mifflin, A. L.; Musorrafiti, M. J.; Geiger, F. M., Kinetic Studies of Chromium (VI) Binding to Carboxylic Acid- and Methyl Ester-Functionalized Silica/Water Interfaces Important in Geochemistry. *J. Phys. Chem. B* **2005,** *109*.

75. Al-Abadleh, H. A.; Voges, A. B.; Bertin, P. A.; Nguyen; Geiger, F. M., Chromium(VI) Binding to Functionalized Silica/Water Interfaces Studied by Nonlinear Optical Spectroscopy. *J. Am. Chem. Soc.* **2004,** *126* (36), 11126-11127.

76. Azam, M. S. G.-D., J. M., Monitoring DNA Hybridization and Thermal Dissociation at the Silica/Water Interface Using Resonantly Enhanced Second Harmonic Generation Spectroscopy. *Anal. Chem.* **2013,** *85* (17), 8031-8038.

77. Fisk, J. D.; Batten, R.; Jones, G.; O'Reill, J. P.; Shaw, A. M., pH Dependence of the Crystal Violet Adsorption Isotherm at the Silica/Water Interface. *J. Phys. Chem. B* **2005,** *109* (30), 14475-14480.

78. Fisk, J. D.; O'Reilly, J. P.; Shaw, A. M., Reply to "Comment on 'Interfacial pH of an Isolated Silica-Water Interface'". *J. Phys. Chem. B* **2006,** *110*, 15039-15040.

79. Hertl, W.; Hair, M. L., Adsorption of Water on Silica. *Nat.* **1969,** *223* (5211), 1150-1151.

80. Isaienko, O.; Borguet, E., Hydrophobicity of Hydroxylated Amorphous Fused Silica Surfaces. *Langmuir* **2013,** *29* (25), 7885-7895.

81. Jordan, D. S.; Malin, J. N.; Geiger, F. M., Interactions of Al(III), La(III), Gd(III), and Lu(III) with the Fused Silica/Water Interface Studied by Second Harmonic Generation. *Environ. Sci. Technol.* **2010,** *44* (15), 5862-5867.

82. Konek, C. T.; Musorrafiti, M. J.; Al-Abadleh, H. A.; Bertin, P. A.; Nguyen, S. T.; Geiger, F. M., Interfacial Acidities, Charge Densities, Potentials, and Energies of Carboxylic Acid-

Functionalized Silica/Water Interfaces Determined by Second Harmonic Generation. *J. Am. Chem. Soc.* **2004,** *126*, 11754-11755.

83. Myalitsin, A.; Urashima, S.-h.; Nihonyanagi, S.; Yamaguchi, S.; Tahara, T., Water Structure at the Buried Silica/Aqueous Interface Studied by Heterodyne-Detected Vibrational Sum-Frequency Generation. *J. Phys. Chem. C* **2016,** *120* (17), 9357-9363.

84. O'Reilly, J. P.; Butts, C. P.; I'Anson, I. A.; Shaw, A. M., Interfacial pH at an Isolated Silica-Water Surface. *J. Am. Chem. Soc.* **2005,** *127*, 1632-1633.

85. Salis, A.; Parsons, D. F.; Bostrom, M.; Medda, L.; Barse, B.; Ninham, B. W.; Monduzzi, M., Ion Specific Surface Charge Density of SBA-15 Mesoporous Silica. *Langmuir* **2010,** *26* (4), 2484-2490.

86. Sulpizi, M.; Gaigeot, M.-P.; Sprik, M., The Silica–Water Interface: How the Silanols Determine the Surface Acidity and Modulate the Water Properties. *J. Chem. Theory Comput.* **2012,** *8* (3), 1037-1047.

87. Bard, A. J. F., L.R.;, Electrochemical Methods: Fundamentals and Applications. *John Wiley and Sons* **2001,** *2nd ed.*

88. Scales, P. J.; Grieser, F.; Healy, T. W.; White, L. R.; Chan, D. Y. C., Electrokinetics of the silica-solution interface: a flat plate streaming potential study. *Langmuir* **1992,** *8* (3), 965-974.

89. Sotira, Y.; Tien, C., *Kinetics of Metal Ion Adsorption from Aqueous Solutions*. Springer US: 1995.

90. Hopkins, A. J.; Schrödle, S.; Richmond, G. L., Specific Ion Effects of Salt Solutions at the CaF2/Water Interface. *Langmuir* **2010,** *26* (13), 10784-10790.

91. Romero-Vargas Castrillón, S.; Giovambattista, N.; Aksay, I. A.; Debenedetti, P. G., Effect of Surface Polarity on the Structure and Dynamics of Water in Nanoscale Confinement. *J. Phys. Chem. B* **2009,** *113* (5), 1438-1446.

92. Ostroverkhov, V.; Waychunas, G.; Shen, Y., New Information on Water Interfacial Structure Revealed by Phase-Sensitive Surface Spectroscopy. *Phys. Rev. Lett.* **2005,** *94* (4).

93. Ostroverkhov, V.; Waychunas, G. A.; Shen, Y. R., Vibrational spectra of water at water/α-quartz (0 0 0 1) interface. *Chem. Phys. Lett.* **2004,** *386* (1–3), 144-148.

94. Covert, P. A. H., D. K., Geochemical Insight from Nonlinear Optical Studies of Mineral–Water Interfaces. *Annu. Rev. Phys. Chem.* **2016,** *67* (1), 233-257.

95. Dewan, S.; Mohsen S. Yeganeh; Borguet, E., Experimental Correlation Between Interfacial Water Structure and Mineral Reactivity. *J. Phys. Chem. Lett.* **2013,** *4*, 1977-1982.

96. Jena, K. C.; Covert, P. A.; Hore, D. K., The Effect of Salt on the Water Structure at a Charged Solid Surface: Differentiating Second- and Third-order Nonlinear Contributions. *J. Phys. Chem. Lett.* **2011,** *2* (9), 1056-1061.

97. Lovering, K. A.; Bertram, A. K.; Chou, K. C., New Information on the Ion-Identity-Dependent Structure of Stern Layer Revealed by Sum Frequency Generation Vibrational Spectroscopy. *J. Phys. Chem. C* **2016,** *120* (32), 18099-18104.

98. Dewan, S.; Carnevale, V.; Bankura, A.; Eftekhari-Bafrooei, A.; Fiorin, G.; Klein, M. L.; Borguet, E., Structure of Water at Charged Interfaces: A Molecular Dynamics Study. *Langmuir* **2014,** *30* (27), 8056-8065.

99. Du, Q.; Freysz, E.; Shen, Y. R., Vibrational spectra of water molecules at quartz/water interfaces. *Phys. Rev. Lett.* **1994,** *72* (2), 238-241.

100. Papirer, E., *Adsorption on Silica Surfaces*. 2000; Vol. 90.

101. Vakarelski, I. U.; Ishimura, K.; Higashitani, K., Adhesion between Silica Particle and Mica Surfaces in Water and Electrolyte Solutions. *J. Coll. Interf. Sci.* **2000,** *227* (1), 111-118.

102. Franks, G. V., Zeta Potentials and Yield Stresses of Silica Suspensions in Concentrated Monovalent Electrolytes: Isoelectric Point Shift and Additional Attraction. *J. Coll. Interf. Sci.* **2002,** *249* (1), 44-51.

103. Sverjensky, D. A., Interpretation and prediction of triple-layer model capacitances and the structure of the oxide–electrolyte–water interface. *Geochim. Cosmochim. Acta* **2001,** *65* (21), 3643-3655.

104. Donose, B. C.; Vakarelski, I. U.; Higashitani, K., Silica Surfaces Lubrication by Hydrated Cations Adsorption from Electrolyte Solutions. *Langmuir* **2005,** *21* (5), 1834-1839.

105. Chapel, J. P., Electrolyte Species Dependent Hydration Forces between Silica Surfaces. *Langmuir* **1994,** *10* (11), 4237-4243.

106. Tadros, T. F.; Lyklema, J., Adsorption of potential-determining ions at the silica-aqueous electrolyte interface and the role of some cations. *J. Electroanal. Chem. Interfacial Electrochem.* **1968,** *17* (3), 267-275.

107. Hocine, S.; Hartkamp, R.; Siboulet, B.; Duvail, M.; Coasne, B.; Turq, P.; Dufrêche, J.-F., How Ion Condensation Occurs at a Charged Surface: A Molecular Dynamics Investigation of the Stern Layer for Water–Silica Interfaces. *J. Phys. Chem. C* **2016,** *120* (2), 963-973.

108. Eisenthal, K. B., Liquid interfaces probed by second-harmonic and sum-frequency spectroscopy. *Chem. Rev.* **1996,** *96* (4), 1343-1360.

109. Kosmulski, M., Positive Electrokinetic Charge of Silica in the Presence of Chlorides. *J. Coll. Interf. Sci.* **1998,** *208* (2), 543-545.

110. Jena, K. C.; Hore, D. K., Variation of Ionic Strength Reveals the Interfacial Water Structure at a Charged Mineral Surface. *J. Phys. Chem. C* **2009,** *113* (34), 15364-15372.

111. Mähler, J.; Persson, I., A Study of the Hydration of the Alkali Metal Ions in Aqueous Solution. *Inorg. Chem.* **2012,** *51* (1), 425-438.

112. Schultz, Z. D.; Shaw, S. K.; Gewirth, A. A., Potential Dependent Organization of Water at the Electrified Metal−Liquid Interface. *J. Am. Chem. Soc.* **2005,** *127* (45), 15916-15922.

113. Kosmulski, M., Positive Electrokinetic Charge of Silica in the Presence of Chlorides. *J. Colloid. Interf. Sci.* **1998,** *208* (2), 543-545.

114. Khatib, R.; Backus, E. H.; Bonn, M.; Perez-Haro, M. J.; Gaigeot, M. P.; Sulpizi, M., Water orientation and hydrogen-bond structure at the fluorite/water interface. *Sci. Rep.* **2016,** *6*, 24287.

115. Kumar, R.; Keyes, T., The relation between the structure of the first solvation shell and the IR spectra of aqueous solutions. *J. Biol. Phys.* **2012,** *38* (1), 75-83.

116. Hocine, S.; Hartkamp, R.; Siboulet, B.; Duvail, M.; Coasne, B.; Turq, P.; Dufrêche, J.-F., How Ion Condensation Occurs at a Charged Surface: A Molecular Dynamics Investigation of the Stern Layer for Water–Silica Interfaces. *J. Phys. Chem. C* **2016,** *120* (2), 963-973.

117. Appelo, C. A. J.; Postma, D., *Geochemistry, Groundwater and Pollution*. 2 ed.; A. A. Balkema Publishers: Amsterdam, 2005.

118. Deutsch, W. J. S., R., *Groundwater Geochemistry: fundamentals and applications to contamination*. CRC Press: Boca Raton, Florida, 1997.

119. Pradeep, K.; Nepolian, M.; Anandhan, P.; Chandran; Kaviyarasan, R.; Prasanna, M. V.; Chidambaram, S., A study on variation in dissolved silica concentration in groundwater of hard rock aquifers in Southeast coast of India. *Mat. Sci. Eng.* **2016,** *121* (1), 012008.

120. Kerian, E. L. D. K., S.; Azam, M.S.; Zeng, H.; Liu, Q.; Gibbs, J.M.;, pH-Dependent Inversion of Hofmeister Trends in the Water Structure of the Electrical Double Layer. *J. Phys. Chem. Lett.* **2017,** 2855-2861.

121. Mackenzie, F. T.; Garrels, R. M., Silica-bicarbonate balance in the ocean and early diagenesis. *J. Sediment. Res.* **1966,** *36* (4), 1075-1084.

122. Pittwell, L. R., The solubility of silica in carbonate waters. *J. Hydroi.* **1974,** *21* (3), 299-300.

123. Kotlyar, L. S.; Sparks, B. D.; Schutte, R., Role of bicarbonate ions in the stability of ultra-fines suspensions. *Environ. Sci. Technol.* **1995,** *30* (6), 1277-1288.

124. Nagarajah, S.; Posner, A. M.; Quirk, J. P., Desorption of Phosphate from Kaolinite by Citrate and Bicarbonate. *Soil Sci. Soc. Am. Proc.* **1968,** *32* (4), 507-510.

125. Ozdemir, O.; Çelik, M. S.; Nickolov, Z. S.; Miller, J. D., Water structure and its influence on the flotation of carbonate and bicarbonate salts. *J. Coll. Interf. Sci.* **2007,** *314* (2), 545-551.

126. Ozdemir, O.; Karakashev, S. I.; Nguyen, A. V.; Miller, J. D., Adsorption of carbonate and bicarbonate salts at the air–brine interface. *Int. J. Miner. Process.* **2006,** *81* (3), 149-158.

127. Du, H.; Liu, J.; Ozdemir, O.; Nguyen, A. V.; Miller, J. D., Molecular features of the air/carbonate solution interface. *Journal of Colloid and Interface Science* **2008,** *318* (2), 271-277.

128. Hannam, K. D.; Kehila, D.; Millard, P.; Midwood, A. J.; Neilsen, D.; Neilsen, G. H.; Forge, T. A.; Nichol, C.; Jones, M. D., Bicarbonates in irrigation water contribute to carbonate formation and CO2 production in orchard soils under drip irrigation. *Geoderma* **2016,** *266*, 120-126.

129. Hua, W.; Chen, X.; Allen, H. C., Phase-Sensitive Sum Frequency Revealing Accommodation of Bicarbonate Ions, and Charge Separation of Sodium and Carbonate Ions within the Air/Water Interface. *J. Phys. Chem. A* **2011,** *115* (23), 6233-6238.

130. Nickolov, Z. S.; Miller, J. D., Water structure in aqueous solutions of alkali halide salts: FTIR spectroscopy of the OD stretching band. *J. Coll. Interf. Sci.* **2005,** *287* (2), 572-580.

131. Du, H.; Liu, J.; Ozdemir, O.; Nguyen, A. V.; Miller, J. D., Molecular features of the air/carbonate solution interface. *J. Coll. Interf. Sci.* **2008,** *318* (2), 271-277.

132. Werner, S. M., J. J., *Aquatic Chemistry: Chemical Equilibria and Rates in Natural Waters; Third Edition*. Wiley: 1995; p 1022 pp.

133. Drever, J. I., *The geochemistry of natural waters : surface and groundwater environments*. 3rd ed. ed.; Prentice Hall: Upper Saddle River, N.J. :, 1997.

134. Faust, S. D.; Aly, O. M., *Chemistry of natural waters*. Ann Arbor Science Publishers: 1981.